NBSIR 73-128

AFCRL-TR-73-0107

RESISTIVITY AND CARRIER LIFETIME IN GOLD-DOPED SILICON

by

W. Robert Thurber, David C. Lewis, and W. Murray Bullis

Electronic Technology Division
Institute for Applied Technology
National Bureau of Standards
Washington, D. C. 20234

PRO Y-72-873
Project No. 6096
Task No. 609604
Work Unit No. 60960401

FINAL REPORT

Period Covered: 1 January 1972 - 31 December 1972

January 31, 1973

Contract Monitor: D. Eirug Davies, Solid State Sciences Laboratory

Approved for public release; distribution unlimited.

Prepared
for

AIR FORCE CAMBRIDGE RESEARCH LABORATORIES
AIR FORCE SYSTEMS COMMAND
UNITED STATES AIR FORCE
BEDFORD, MASSACHUSETTS 01730

AFCRL-TR-73-0107

RESISTIVITY AND CARRIER LIFETIME IN GOLD-DOPED SILICON

by

W. Robert Thurber, David C. Lewis, and W. Murray Bullis

Electronic Technology Division
Institute for Applied Technology
National Bureau of Standards
Washington, D. C. 20234

PRO Y-72-873
Project No. 6096
Task No. 609604
Work Unit No. 60960401

FINAL REPORT

Period Covered: 1 January 1972 - 31 December 1972

January 31, 1973

Contract Monitor: D. Eirug Davies, Solid State Sciences Laboratory

Approved for public release; distribution unlimited.

Prepared
for

AIR FORCE CAMBRIDGE RESEARCH LABORATORIES
AIR FORCE SYSTEMS COMMAND
UNITED STATES AIR FORCE
BEDFORD, MASSACHUSETTS 01730

Qualified requestors may obtain additional copies from
the Defense Documentation Center. All others should
apply to the National Technical Information Service.

ABSTRACT

This report describes the current status of a continuing study of the electrical properties of gold-doped silicon. Room temperature resistivity and Hall effect measurements were made on many sets of gold-diffused, boron- or phosphorus-doped silicon wafers for a wide range of initial resistivities of both types. The general suitability of the proposed model was verified although an apparent discrepancy still remains between total and electrically active gold as confirmed by resistivity data as a function of gold density for phosphorus-doped silicon. Electrical measurements were made to study the activation energies of the gold donor and acceptor. In addition the activation energy of the gold-coupled shallow acceptor in the proposed model was observed. The values found were in good agreement with other reported observations of these levels. In the application of the surface photovoltage method to the measurement of minority carrier lifetime, it was found that the optical absorption coefficients needed in the analysis of the data were dependent on the heat treatment given to the specimen. The uncertainty in diffusion length was determined to be about 2 μm which placed an effective lower limit on lifetime measurements of about 15 ns in *p*-type and about 50 ns in *n*-type silicon. An analysis of the use of the surface photovoltage method for lifetime measurements in thin epitaxial layers is included as an appendix. The reverse recovery (RR) technique for measuring lifetime was examined and it was observed that the dependence of diode storage time on the ratio of forward to reverse current varied with the base width of the diode studied. While theory and experiment for open circuit voltage decay (OCVD) were in agreement for long base width diodes, correlation for short base diodes was less satisfactory; this study is continuing. Both the RR and OCVD techniques give the same value of lifetime for long base diodes, but agreement for short base diodes is not as good. Additional entries are included as a supplement to an earlier bibliography on the properties of gold-doped silicon.

CONTENTS

PAGE

Foreword vi

Introduction 1

Specimen Preparation and Determination of Gold Density . . . 3

Resistivity and Hall Effect Measurements 5

Resistivity vs. Gold Density in p-Type Silicon 5
Resistivity vs. Gold Density in n-Type Silicon 8
Activation Energies 14
Carrier Mobility 23
Heat Treatment Studies 23

Carrier Lifetime Measurements 27

Surface Photovoltage Method 27
Diode Recovery Methods 28
Reverse Recovery Method 29
Open Circuit Voltage Decay Method 32
Comparisons Between RR and OCVD Measurements 34

Directions for Future Work 35

References 37

Appendix A — Specimen Preparation 39

Appendix B — Activation Analysis 41

Appendix C — Interpretation of Steady-State Surface Photovoltage Measurements in Epitaxial Semiconductor Layers 43

Appendix D — Supplementary Bibliography: Gold-Doped Silicon 49

FOREWORD

The work reported here is a part of the Joint Program on Methods of Measurement for Semiconductor Materials, Process Control, and Devices. This program is carried out at the National Bureau of Standards and receives support from a number of other agencies of the Federal Government in addition to the NBS. The program was undertaken in 1968 to focus NBS efforts to enhance the performance, interchangeability, and reliability of discrete semiconductor devices and integrated circuits through improvements in methods of measurement for use in specifying materials and devices and in control of device fabrication processes. These improvements are intended to lead to a set of measurement methods which have been carefully evaluated for technical adequacy, which are acceptable to both users and suppliers, which can provide a common basis for the purchase specifications of government agencies, and which will lead to greater economy in government procurement. In addition, such methods will provide a basis for controlled improvements in essential device characteristics, such as uniformity of response to radiation effects. During 1972 the portion of the program concerned with gold-doped silicon received partial support from the Air Force Cambridge Research Laboratories (LQD) under project order Y-72-873. The contract monitor was D. E. Davies. The present project is a follow-on to AFCRL PRO Y-71-906.

Technical personnel who contributed to this effort during the period covered were:

W. M. Bullis, supervisory physicist, principal investigator
M. Cosman, mechanical engineering technician, specimen preparation
T. E. Gills, research chemist, neutron activation analysis
J. Krawczyk, physical science technician, diffusion
T. F. Leedy, physicist, diffusion
D. C. Lewis, general physical scientist, diode recovery measurements and analysis
W. E. Phillips, physicist, surface-photovoltage measurements
P. M. Sandow, general physical scientist, spreading resistance measurements
A. W. Stallings, mechanical engineering technician, electrical measurements
W. R. Thurber, physicist, electrical measurements

Preliminary reports of the work have been reported in Joint Program quarterly progress reports that have been issued in the NBS Technical Note series. NBS Technical Notes 733, 743, and 754 cover periods during which support was received under the above noted project order. Earlier work is reported in NBS Technical Notes 488, 495, 520, 527, 560, 571, 592, 598, 702, 717, and 727.

RESISTIVITY AND CARRIER LIFETIME IN GOLD-DOPED SILICON

W. Robert Thurber, David C. Lewis, and W. Murray Bullis

INTRODUCTION

Gold is an amphoteric recombination center in silicon. Its addition to either *n*-type or *p*-type silicon will affect the carrier lifetime. No other impurity addition has been found that is as effective for controlling carrier lifetime in silicon; hence, gold is widely used in device fabrication.

The basic electrical model for the impurity states associated with gold was clearly enunciated in early work on gold-doped silicon [1], and the diffusion technology for introducing gold into the silicon lattice, though largely empirical, is under sufficient control that device manufacturers can successfully employ it on a large-scale. Nevertheless, unresolved problems remain in both areas. In particular, clarification of the details of the electrical model is necessary before concentrations of gold centers can be determined unambiguously from measurements of resistivity or carrier lifetime as might be desired, for example, in before-and-after studies of radiation effects in gold-doped silicon.

In the work reported here, reasons are being sought for the apparent discrepancy between total and electrically active gold, for the discrepancy between calculated and observed resistivity in both *n*-type and *p*-type specimens with very large gold concentration, and for the diversity in the capture cross section data reported in the literature. To investigate these problems, a series of silicon wafers to which various amounts of gold and phosphorus or boron have been added is being characterized by measuring resistivity, Hall coefficient, and carrier lifetime at room temperature. Gold concentrations are determined directly by neutron activation analysis after gold has been diffused into the wafer; shallow dopant (phosphorus or boron) concentrations are determined by measurement of wafer resistivity before gold diffusion. In addition, ancillary experiments and computations to develop the diffusion technology necessary to prepare the specimens and to elucidate certain aspects of proposed models are being carried out.

In earlier phases of this work [2], specimen preparation, electrical measurement, and activation analysis procedures were established. From electrical measurements on a limited range of specimens, a model was identified that appeared to account for the observed resistivity of *p*-type silicon heavily doped with gold. In addition the surface photovoltage technique for measuring minority carrier diffusion length was studied extensively. Two difficulties were encountered in applying this technique to gold-doped silicon specimens. First, the uncertainty in diffusion length was found to be about 1 or 2 μm which placed an effective lower limit on lifetime measurements of about 15 ns in *p*-type silicon and about 50 ns in *n*-type silicon. Second, the optical absorption coefficient data needed in the analysis of the measurements was dependent on the heat treatment given to the specimen.

During the period covered by the present report the electrical studies were almost completed and the general suitability of the proposed model was confirmed. Additional analysis of the data was undertaken to seek an explanation for the apparent discrepancy between total and electrically active gold, but no satisfactory result was obtained. Electrical measurements were also studied to obtain the energy levels of the gold donor and acceptor. In addition, the energy level of the gold-coupled shallow acceptor in the proposed model was also observed, confirming the result reported by Brückner [3].

Additional studies of the steady-state surface photovoltage (SPV) method were conducted with particular emphasis on the problems of accurate absorption coefficient data and of experimental reproducibility for short diffusion length measurements. A detailed analysis of the application of the SPV method to measurements in thin epitaxial layers was completed and published. Because of the limitations of this method for measurement of short lifetimes, attention was redirected toward reverse recovery and open circuit voltage decay measurements. Considerable insight into the previously observed discrepancies between these methods has been developed in this study which is still underway.

SPECIMEN PREPARATION AND DETERMINATION OF GOLD DENSITY

Both *n*-type and *p*-type crystals doped with phosphorus and boron, respectively are being studied. About ten resistivity values of each type cover the range 0.01 to 2500 Ω·cm as listed in table 1. Specimens were prepared for electrical measurements and gold density determinations in essentially the same manner as used during the previous work [2]. Details are given in Appendix A.

Gold densities were determined by neutron activation analysis by the second of the two procedures described previously [2]. Details are given in Appendix B.

Table 1 — Silicon Crystals for Gold Diffusion

Initial Resistivity ρ_i, $\Omega\cdot$cm	Type	Pulled or Float Zoned	Status
∿0.01	*n*	f-z	available
∿0.01	*p*	f-z	available
∿0.08	*n*	pulled	available
0.076	*p*	pulled	measured
0.30	*n*	f-z	measured
0.53	*p*	pulled	measured
1.0	*n*	f-z	measured
1.1	*p*	pulled	measured
5.3	*n*	pulled	measured
11	*p*	pulled	measured
∿20	*n*	f-z	available
20	*p*	f-z	measured
75	*n*	f-z	measured
93	*p*	f-z	measured
380	*n*	f-z	measured
280	*p*	f-z	measured
∿1000	*n*	f-z	available
1100	*p*	f-z	measured
2300	*n*	f-z	measured
2300	*p*	f-z	measured
2700	*p*	pulled	measured

Resistivity vs. Gold Density in p-Type Silicon — During this period, resistivity measurements were made on boron-doped silicon wafers with initial room-temperature resistivities (before the addition of gold) of 0.076, 0.53, 1.1, 280, 1100, 2300, and 2700 Ω·cm. The gold density ranged from about 10^{14} cm^{-3} to about 10^{17} cm^{-3}. The resistivity of these, and previously measured initially 11-, 20-, and 93-Ω·cm specimens, is shown as a function of gold density in figures 1 and 2.

Theoretical curves, generated for comparison of the experimental resistivity data as a function of gold density with predictions of the energy-level model for gold-doped silicon, are also shown in figures 1 and 2. The curves were derived from calculations based on a solution to the charge balance equation

$$n + N_a^- + N_G^- + N_A^- = p + N_d^+ + N_D^+ \qquad (1)$$

where, for the non-degenerate case of interest here:

$n \approx N_c \exp[(F - E_c)/kT]$ is the electron density,

$p \approx N_v \exp[(E_v - F)/kT]$ is the hole density,

$N_c = 2(2\pi m_e kT/h^2)^{3/2}$ is the density of states in the conduction band,

$N_v = 2(2\pi m_h kT/h^2)^{3/2}$ is the density of states in the valence band,

$N_a^- = N_a/\{1 + g_a \exp[(E_a - F)/kT]\}$ is the ionized (filled) shallow acceptor (boron, etc.) density,

$N_G^- = N_G/\{1 + g_G \exp[(E_G - F)/kT]\}$ is the ionized (filled) gold-coupled shallow acceptor density,

$N_A^- = N_{Au}/(1 + g_A \exp[(E_A - F)/kT]\{1 + g_D \exp[(E_D - F)/kT]\})^{-1}$ is the density of negatively ionized gold (filled acceptors),

$N_d^+ = N_d/\{1 + g_d^{-1} \exp[(F - E_d)/kT]\}$ is the ionized (empty) shallow donor (phosphorus, etc.) density,

$N_D^+ = N_{Au}/(1 + g_D^{-1} \exp[(F - E_D)/kT]\{1 + g_A^{-1} \exp[(F - E_A)/kT]\})^{-1}$ is the density of positively ionized gold (empty donors),

m_e, m_h are the electron and hole effective masses,

k is Boltzmann's constant,

T is absolute temperature,

h is Planck's constant,

F is the Fermi energy,

E_c, E_v are the energies of the conduction and valence band edges,

N_a, N_G, N_{Au}, N_d are the densities of shallow acceptors, gold-coupled shallow acceptors, gold, and shallow donors,

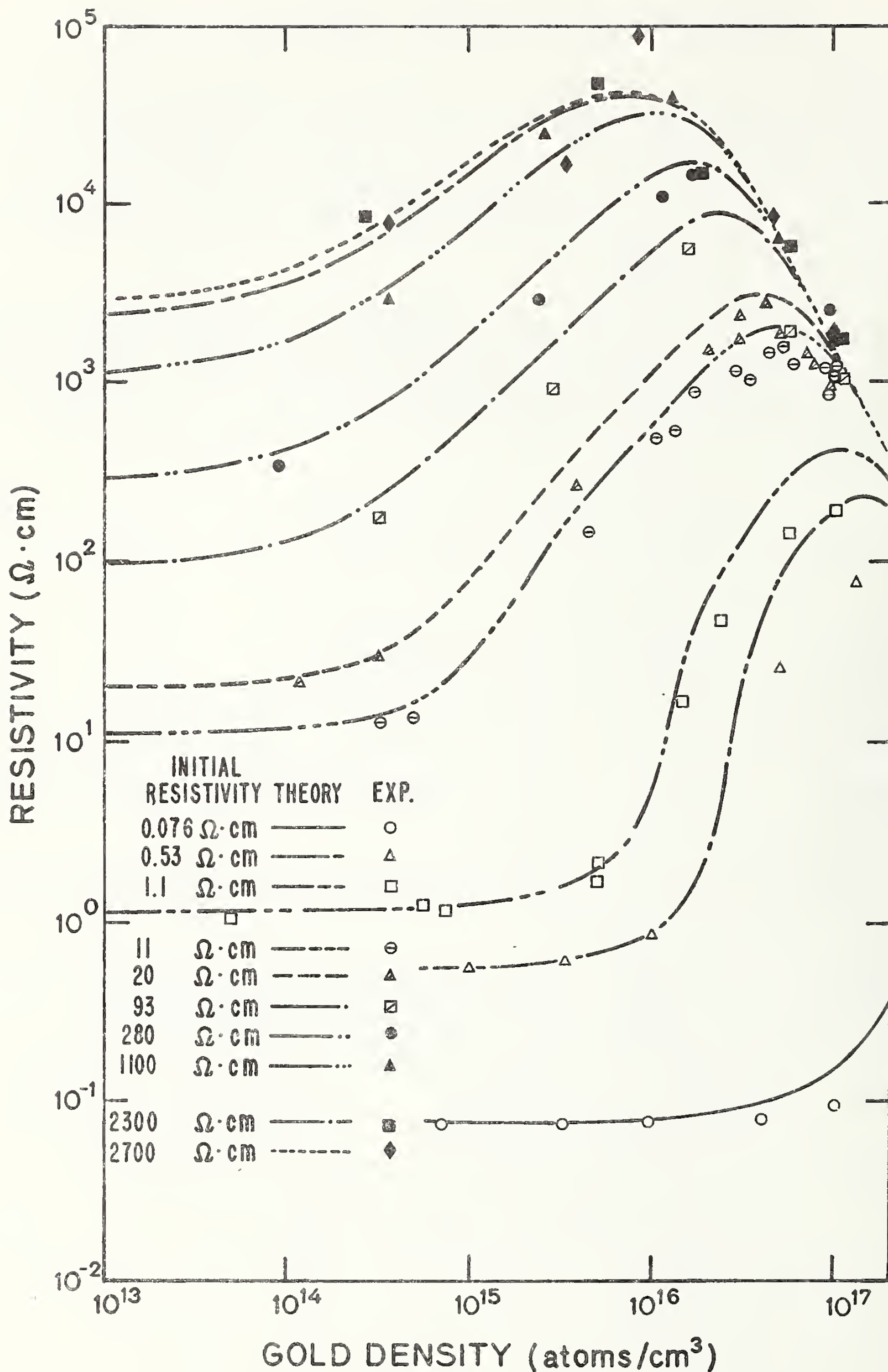

Figure 1. Resistivity as a function of gold density in boron-doped silicon assuming the degeneracy factor of the gold donor level to be 8.

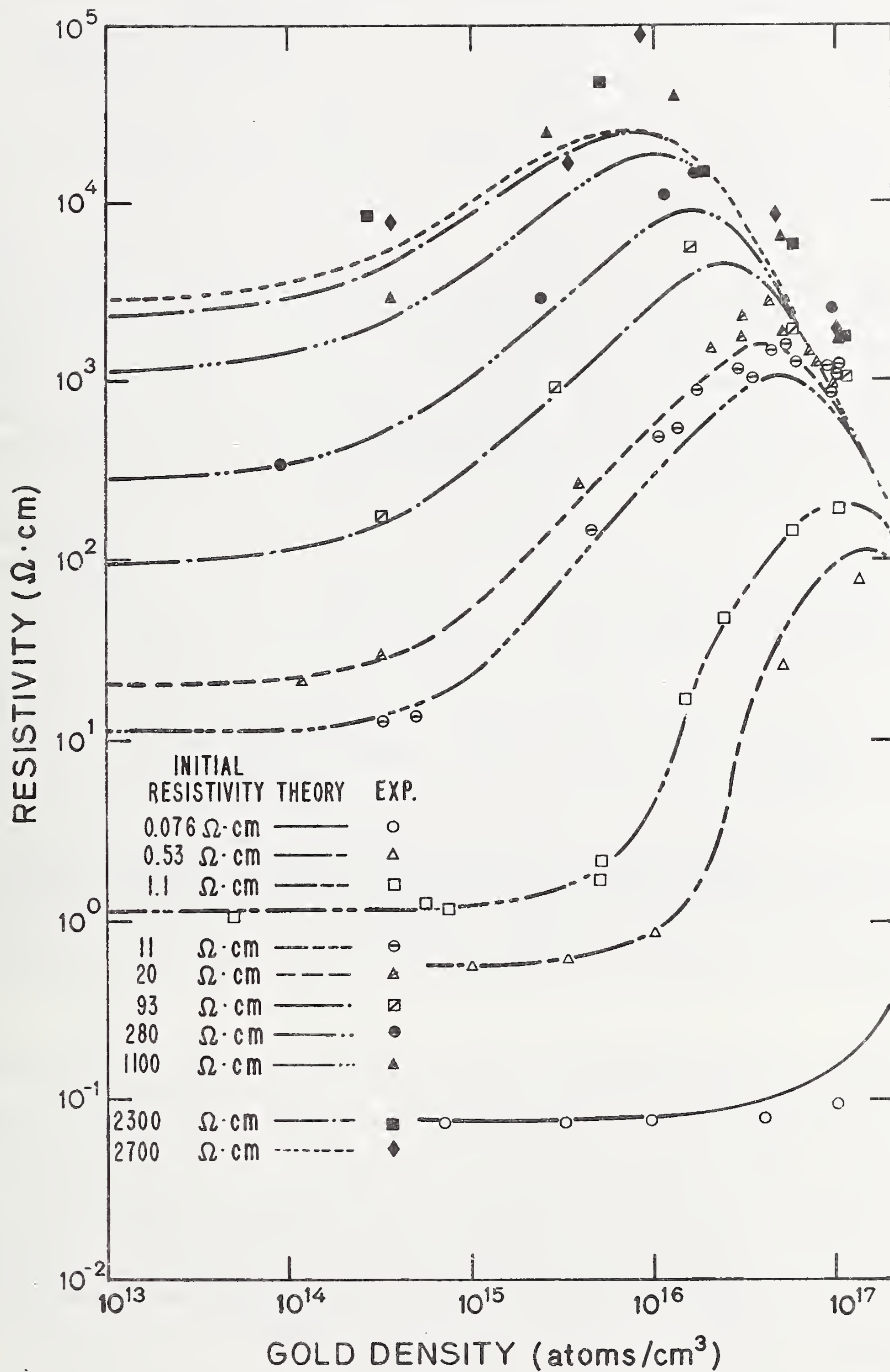

Figure 2. Resistivity as a function of gold density in boron-doped silicon assuming the degeneracy factor of the gold donor level to be 16.

g_a, g_G, g_A, g_D, g_d are the degeneracy factors* of the shallow acceptor, the gold-coupled shallow acceptor, the gold acceptor, the gold donor, and the shallow donor, and

E_a, E_G, E_A, E_D, E_d are the energies of the shallow acceptor, the gold-coupled shallow acceptor, the gold acceptor, the gold donor, and the shallow donor.

For the assumed model, shown in figure 3, T = 298 K; $E_D - E_V = 0.35$ eV and $E_A - E_V = 0.58$ eV [1]; $E_c - E_V = 1.111$ eV [5], $m_e = 1.18\ m_o$ [6], and $m_h = 0.81\ m_o$ [6] (m_o = the free electron mass), so $n_i = \sqrt{np} = 9.6 \times 10^9\ \text{cm}^{-3}$. The lattice mobility [7] and impurity mobility [8] were combined reciprocally to obtain the carrier mobility used in the calculation of the resistivity. Also included was the gold-coupled acceptor located at 0.033 eV above the valence band [3]. Its dependence on gold density is not well established, but experimental data reported previously [2] suggest that the acceptor density increases approximately as the third power of the gold density with a value of $4.5 \times 10^{15}\ \text{cm}^{-3}$ at a gold density of $1 \times 10^{17}\ \text{cm}^{-3}$. Its degeneracy factor was taken to be 4, the energy and degeneracy factor of the shallow acceptor were taken as 0.045 eV and 4, respectively, values appropriate to boron, and the degeneracy factor of the gold acceptor was taken as $1/8$; none of these values enter significantly into the calculation. Various values of the degeneracy factor for the gold donor were tried to determine which might give the best fit to the experimental data; results for two values, 8 and 16, are shown in figures 1 and 2, respectively. The densities of the shallow acceptor were calculated from eq (1) with the assumption that $N_{Au} = 0$; values are listed in table 2.

Although the calculated curves generally fit the experimental data, there are some deviations which appear to be systematic. Investigations of two possible sources of the deviations, compensation by donor impurities unintentionally introduced during the gold diffusion and the previously observed discrepancy between total and electrically active gold [9], have not yet been completed.

Resistivity vs. Gold Density in n-Type Silicon — Resistivity measurements were made on phosphorus-doped silicon wafers with initial room-temperature resistivities (before the addition of gold) of 0.30 and 1.0 Ω·cm. The gold density ranged from about $10^{14}\ \text{cm}^{-3}$ to about $10^{17}\ \text{cm}^{-3}$. The resistivity of these, and previously measured initially 5.3-, 75-, 380-, and 2300-Ω·cm specimens is shown as a function of gold density in figure 4. At large gold densities, the conductivity type converts from *n* to *p*. Specimens with positive Hall coefficients are plotted with solid symbols in the figure. For the lower resistivities a sharp increase in resistivity is observed when the gold density is between one and two times the density of the shallow donor in agreement with earlier observations [9].

Theoretical curves, based on the energy-level model described above, were calculated for each set of data. The theory predicts that the sharp

---

*The degeneracy factor is defined by Blakemore [4] as referring to the probability that a level contains an electron.

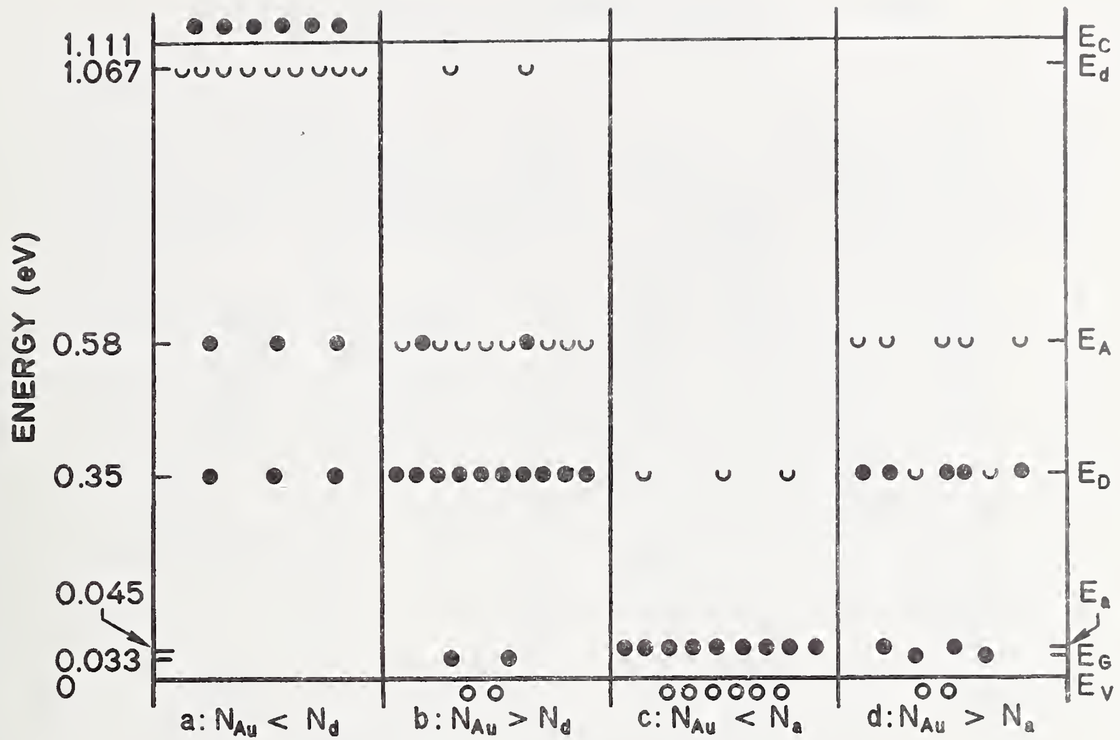

Figure 3. Energy band diagram at 298 K for silicon doped with gold and either phosphorus or boron. In this model it is assumed that the energy differences $E_A - E_c$ and $E_D - E_V$ do not vary with temperature. The energies given for the shallow donor and acceptor levels are appropriate for phosphorus and boron, respectively. No gold-coupled shallow acceptors are shown for cases a and c as their density is negligible when the gold density is less than 10^{16} cm^{-3}.

Table 2 — Doping Densities of Silicon Crystals Computed from Measured Resistivity

p-type		*n*-type	
ρ_i, Ω·cm	N_a, cm^{-3}	ρ_i, Ω·cm	N_d, cm^{-3}
0.076	2.28×10^{17}		
0.53	2.59×10^{16}	0.30	1.60×10^{16}
1.1	1.18×10^{16}	1.0	4.62×10^{15}
11	1.20×10^{15}	5.3	8.60×10^{14}
20	6.55×10^{14}		
93	1.40×10^{14}	75	6.10×10^{13}
280	4.72×10^{13}	380	1.20×10^{13}
1100	1.18×10^{13}		
2300	5.76×10^{12}	2300	2.00×10^{12}
2700	4.80×10^{12}		

Note — The computed doping densities for low resistivity crystals (<1 Ω·cm) shown above are lower than those obtained experimentally [Irvin, J. C., Resistivity of Bulk Silicon and of Diffused Layers in Silicon, *Bell System Tech. J.* 41, 387-410 (1962)]. This discrepancy arises because of difficulties with the calculation of ionized impurity and mixed mobilities.

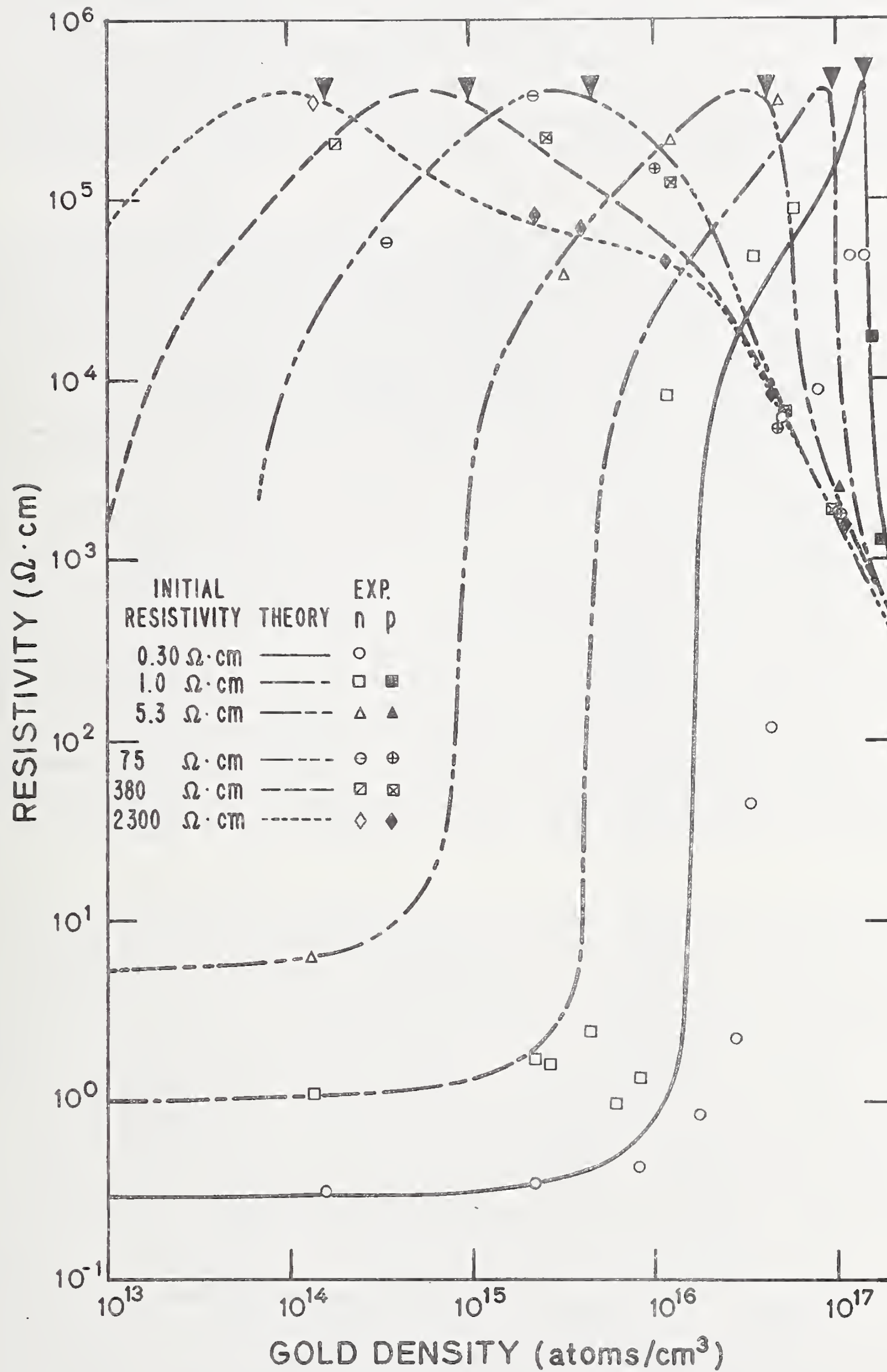

Figure 4. Resistivity as a function of gold density in phosphorus-doped silicon. To the left of the ▼, the Hall coefficient is negative; to the right it is positive.

increase in resistivity will occur when the gold and shallow donor densities are equal. Elsewhere, however, the theoretical and experimental plots have generally similar form. For the curves plotted in figure 4, the energy and degeneracy factor of the shallow donor were taken as 1.067 eV and $1/2$, respectively, the degeneracy factor of the gold acceptor was taken as $1/8$, and the degeneracy factor of the gold donor was taken as 8. Other parameters were chosen as described above; values of shallow donor density, calculated as above, are listed in table 2.

To study the effect of changes in the energy of the gold acceptor and its degeneracy factor on the theoretical fit to the resistivity *vs.* gold density data of the initially 0.3-$\Omega \cdot$cm phosphorus-doped silicon, calculations were made for several values of the acceptor energy and degeneracy factor. The results of these calculations are shown in figure 5. Calculations were made for two energies: 0.54 eV below the conduction band and 0.66 eV above the valence band. These correspond, respectively, to fixing the level to the conduction band and to the valence band for a measured activation energy (energy at 0 K) of 0.54 eV. Because the forbidden energy gap at room temperature is about 1.11 eV rather than about 1.20 eV, fixing the level to the conduction band edge results in a position lower in the gap, 0.57 eV above the valence band edge, than fixing it to the valence band edge. In the latter case, the acceptor level is considerably above mid-gap and the increase in resistivity at near-equal gold and shallow donor densities is much more gradual than for the other case considered. For each value of energy, calculations were made for degeneracy factors of $1/2$, $1/8$, and $1/32$. The degeneracy factor does not affect the position of the sharp rise in resistivity, but it does influence the resistivity at larger gold density where the Fermi level is between the gold donor and the gold acceptor. Since neither of these variables affects the position of the sharp increase, another explanation for the shift must be found before the curves in figure 5 can be fully interpreted.

A suspected cause of the shift was the presence of a significant quantity of interstitial gold with electrical characteristics which compensate those of the substitutional acceptor. To examine the effect of intersititial gold on the electrical properties of silicon, diffusions of short duration were done at 950 and 1150°C in both *n*- and *p*-type wafers to obtain gold densities much lower than the saturation value. Electrical measurements were made on the diffused material and the results compared with data obtained on the same or similar starting material which was diffused to saturation for long times at lower temperatures. The data points for the initially 2300-$\Omega \cdot$cm, *n*-type silicon at the two lowest gold densities in figure 4 were short-time diffusions and are either in agreement with nearby points from long-time diffusions or are close to the calculated curve. In addition, the resistivity data on the *p*-type silicon diffused for short times were in agreement with those obtained on other wafers with the same gold density but diffused for much longer times. Thus the resistivity depends only on the gold density and not on whether saturation was achieved. Schuman [10] studied the electrical characteristics of silicon diffused with gold for short times and concluded that interstitial and substitutional gold affect the electrical properties of silicon in the same manner. The further extension of this conclusion is that interstitial gold is not responsible for the observed shift since the electrical properties would be indistinguishable from those of the substitutional species. This rather surprising similarity need not

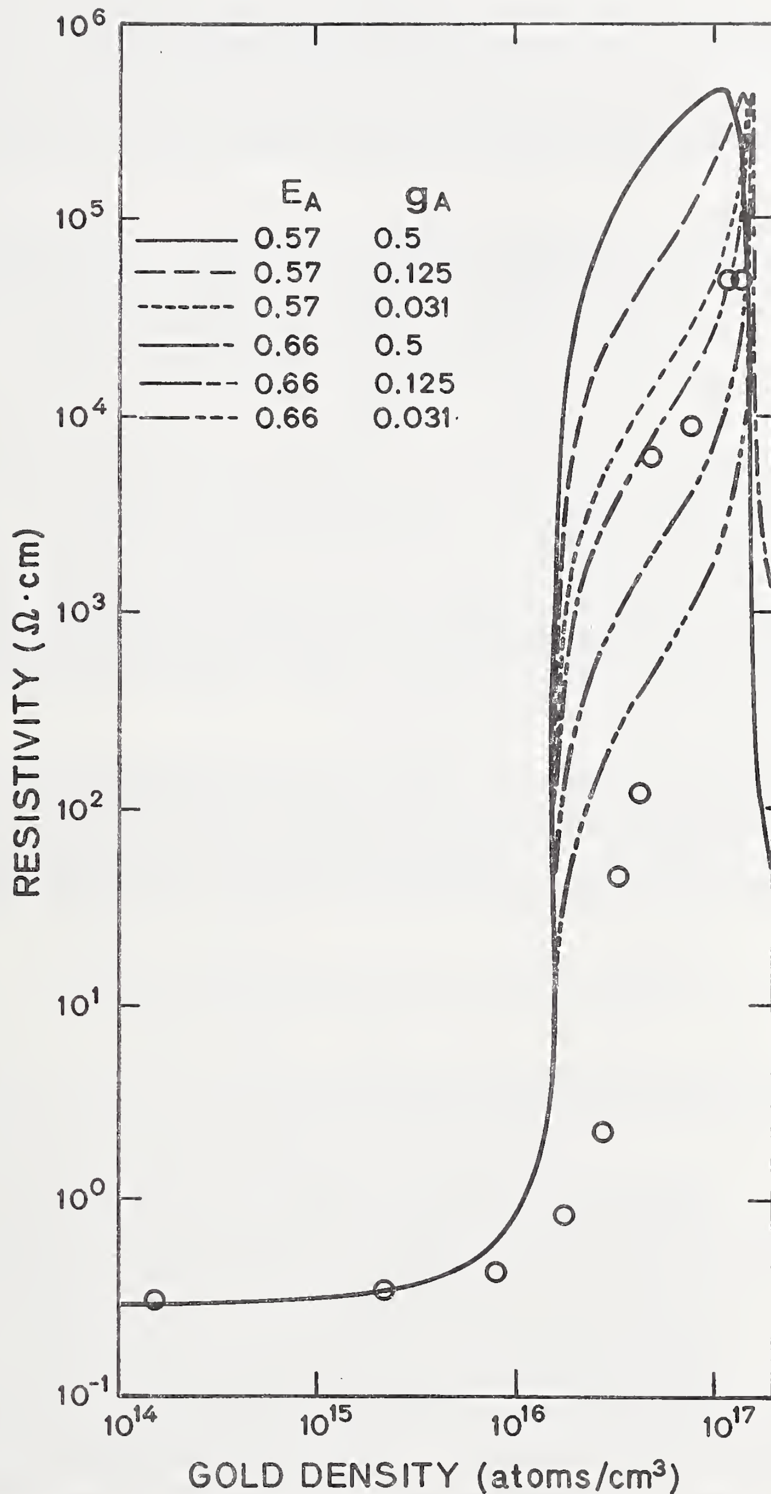

Figure 5. Calculated curves of resistivity as a function of gold density for initially 0.3-Ω·cm, phosphorus-doped silicon. The experimental points are the same as those in figure 4 for the 0.30-Ω·cm silicon.

be invoked if the rate for the conversion of interstitial to substitutional gold is very rapid compared to the diffusion time so that the ratio of substitutional to interstitial gold is independent of diffusion time [11]. In this case, however, the experiment performed cannot discriminate between interstitials and substitutionals since it is not possible to alter their relative densities. At the present time, therefore, it is not possible to rule out the presence of interstitials as being responsible for the observed discrepancy.

Activation Energies — Under certain conditions, eq (1) simplifies and the dominant temperature dependent factor is an exponential which involves the energy of only a single impurity level. The energy level involved is determined by the relative densities of the various impurities.

In *n*-type material with $N_{Au} < N_d$ (case a, figure 3), the electron density is

$$n \approx \frac{N_d - (N_{Au} + N_a)}{N_{Au} + N_a} N_c g_d \exp[-(E_c - E_d)/kT], \tag{2}$$

when $n >> p$, $N_d > N_{Au} + N_a$, $n << N_{Au} + N_a$ and $n << N_d - N_{Au} - N_a$. This is the usual activation energy equation for a partially compensated, shallow donor; it is valid for low temperatures. The Fermi energy is near the shallow donor energy. The density of gold-coupled shallow acceptors under these conditions is small enough to be neglected.

There are three different energies which can control the majority carrier density in initially *n*-type material when $N_{Au} > N_d$ (case b, figure 3). When $n >> p$, $N_d >> N_a + N_G$, $n << N_{Au} + N_a + N_G - N_d$, and $n << N_d - N_a - N_G$, the Fermi energy is near the gold acceptor energy, and the electron density is

$$n \approx \frac{N_d - N_a - N_G}{N_{Au} - (N_d - N_a - N_G)} N_c g_A \exp[-(E_c - E_A)/kT]. \tag{3}$$

In this case the energy difference between the gold acceptor and the conduction band edge governs the electron density.

If the gold density is larger, the specimens become *p*-type (see figure 4) so that $p > n$. Under this condition, where $N_{Au} >> N_d$, $N_a + N_G < N_d$, $p >> n$, $p << N_d - N_a - N_G$, and $p << N_{Au} + N_a + N_G - N_d$, the Fermi energy is near but slightly below the gold acceptor energy, and the hole density is

$$p \approx \frac{N_{Au} - (N_d - N_a - N_G)}{N_d - N_a - N_G} \frac{N_v}{g_A} \exp[-(E_A - E_v)/kT]. \tag{4}$$

In this case the energy difference between the gold acceptor and the valence band edge governs the hole density. This is the case depicted in part b of figure 3.

At still greater gold densities the density of the gold-coupled shallow acceptor becomes significantly larger so that the condition $N_d > N_a + N_G$ no longer holds; instead $N_d < N_a + N_G$ and there are no longer enough electrons

to populate any of the gold acceptors. When $p >> n$, $p << N_a + N_G - N_d$, and $p << N_{Au} + N_d - N_a - N_G$, the hole density is

$$p \approx \frac{N_{Au} - (N_a + N_G - N_d)}{N_a + N_G - N_d} \frac{N_v}{g_D} \exp[-(E_D - E_v)/kT]. \quad (5)$$

In this case the Fermi energy is near the gold donor energy and the energy difference between the gold donor and the valence band edge governs the hole density.

In *p*-type material with $N_{Au} < N_a$ (case c, figure 3), the hole density is

$$p \approx \frac{N_a - (N_{Au} + N_d)}{N_{Au} + N_d} \frac{N_v}{g_a} \exp[-(E_a - E_v)/kT], \quad (6)$$

when $p >> n$, $N_a > N_{Au} + N_d$, $p << N_{Au} + N_d$, and $p << N_a - N_{Au} - N_d$. This is the usual activation energy equation for a partially compensated, shallow acceptor; it is valid at low temperatures. The Fermi energy is near the shallow acceptor energy. Because the density of gold-coupled shallow acceptors is small enough that these levels do not influence the hole density, the energy difference $E_G - E_v$ does not interfere, and only the energy difference $E_a - E_v$ appears in the expression. Note that the gold donor levels are fully ionized (contain no electrons) and that, as a result, the gold acceptor levels do not exist.

In *p*-type material with $N_{Au} > N_a$ (case d, figure 3), there are two different conditions. In the usual case $N_G << N_{Au}$ so, usually, $N_{Au} > N_a + N_G - N_d$. This is the same condition which led to eq (5); the Fermi energy is near the gold donor energy and the energy difference between the gold donor and the valence band edge governs the hole density. If N_{Au} could be reduced such that $N_{Au} < N_a + N_G - N_d$ while $N_G >> N_a$, then the hole density is

$$p \approx \frac{N_G - (N_{Au} + N_d)}{N_{Au} + N_d} \frac{N_v}{g_G} \exp[-(E_G - E_v)/kT]. \quad (7)$$

Brückner [3] found that this condition could be achieved by annealing at 600°C for a short time specimens lightly doped with boron ($N_a \approx 10^{13}$ cm^{-3}) and diffused with gold at ∿1200°C ($N_{Au} \approx 10^{17}$ cm^{-3}).

From eqs (2) through (7) it can be seen that the slope of the linear region of a plot of the logarithm of the majority carrier density, corrected for the temperature dependence of the density of states, N_v or N_c, against reciprocal temperature is proportional to the energy difference between the dominant level and the band edge associated with the majority carrier. The density of states varies directly with the three-halves power of the temperature, T; in addition, the electron and hole effective masses increase slightly with the temperature [6].

If the energy difference is a linear function of temperature

$$\Delta E = \Delta E_o + \beta T,$$

where ΔE_0 is the value of the energy difference at zero kelvin, the temperature dependent term merely introduces the constant factor, ln (β/k), into the expression for carrier density. As a result the value of the energy difference determined from the plot is actually the value linearly extrapolated to zero kelvin. This is called the activation energy.

Activation energies can be obtained from the slopes of the linear portions of either resistivity or Hall coefficient data plotted logarithmically against the reciprocal of the absolute temperature. The activation energy from both plots is slightly incorrect. Error in the case of the resistivity plot arises because the decrease of the mobility with temperature is somewhat greater than the increase of the density of states. Customarily the Hall coefficient, R_H, is multiplied by $T^{1.5}$ to correct for the principal temperature dependence of the density of states. In addition to the effective mass, the scattering factor also contributes a small temperature dependence [12]. Both were neglected in the analysis of the data reported here.

The activation energy of the gold acceptor with respect to the conduction band was obtained from measurements of resistivity and Hall coefficient over the temperature range 200 to 400 K on a specimen of phosphorus-doped silicon with an initial resistivity of 75 Ω·cm and a gold density of 3.6×10^{14} cm^{-3}. Activation energy plots based on resistivity and Hall coefficient data are shown in figures 6 and 7, respectively. In each case the activation energy was calculated from the curves by means of a least squares analysis [13] for the slopes. The data points included in the analysis are shown by circles; the points excluded because of their deviation from linearity are shown as squares. The results are shown in table 3; the uncertainty given for each activation energy is the square root of the estimated variance of the slope of the experimental line.

Activation energy values for the gold donor were obtained from measurements of resistivity and Hall coefficient over the temperature range 140 to 320 K on specimens cut from boron-doped silicon wafers with initial resistivity of 20 Ω·cm and diffused with gold to obtain gold densities of 3.9×10^{15}, 3.1×10^{16}, and 9.9×10^{16} cm^{-3}. Activation energy plots based on resistivity and Hall coefficient data are shown in figures 8 and 9, respectively. The analysis for the activation energies was the same as that used for the gold acceptor; the results are also listed in table 3. Similar values of activation energy were found from resistivity and Hall coefficient data taken on an initially 1100-Ω·cm, boron-doped silicon specimen with a gold density of 1.1×10^{17} cm^{-3} (see table 3).

To expose the shallow, gold-coupled acceptor level [3] in order to measure its activation energy, the initially 1100-Ω·cm, boron-doped specimen was annealed for 1 h at 600°C in a helium atmosphere. After annealing, the room temperature resistivity dropped from 1600 to 14 Ω·cm, and the Hall coefficient, with the assumption of a unity scattering factor, gave a room temperature carrier density of 1.2×10^{15} cm^{-3}, somewhat smaller than the estimated density of the shallow acceptor. This is not unexpected; Brückner [3] found that the shallow acceptor density decreased with annealing, but at a less rapid rate than the density of the electrically active gold donors. Because of high contact resistance, the low temperature Hall data showed considerable scatter, but good resistivity data were obtained over the

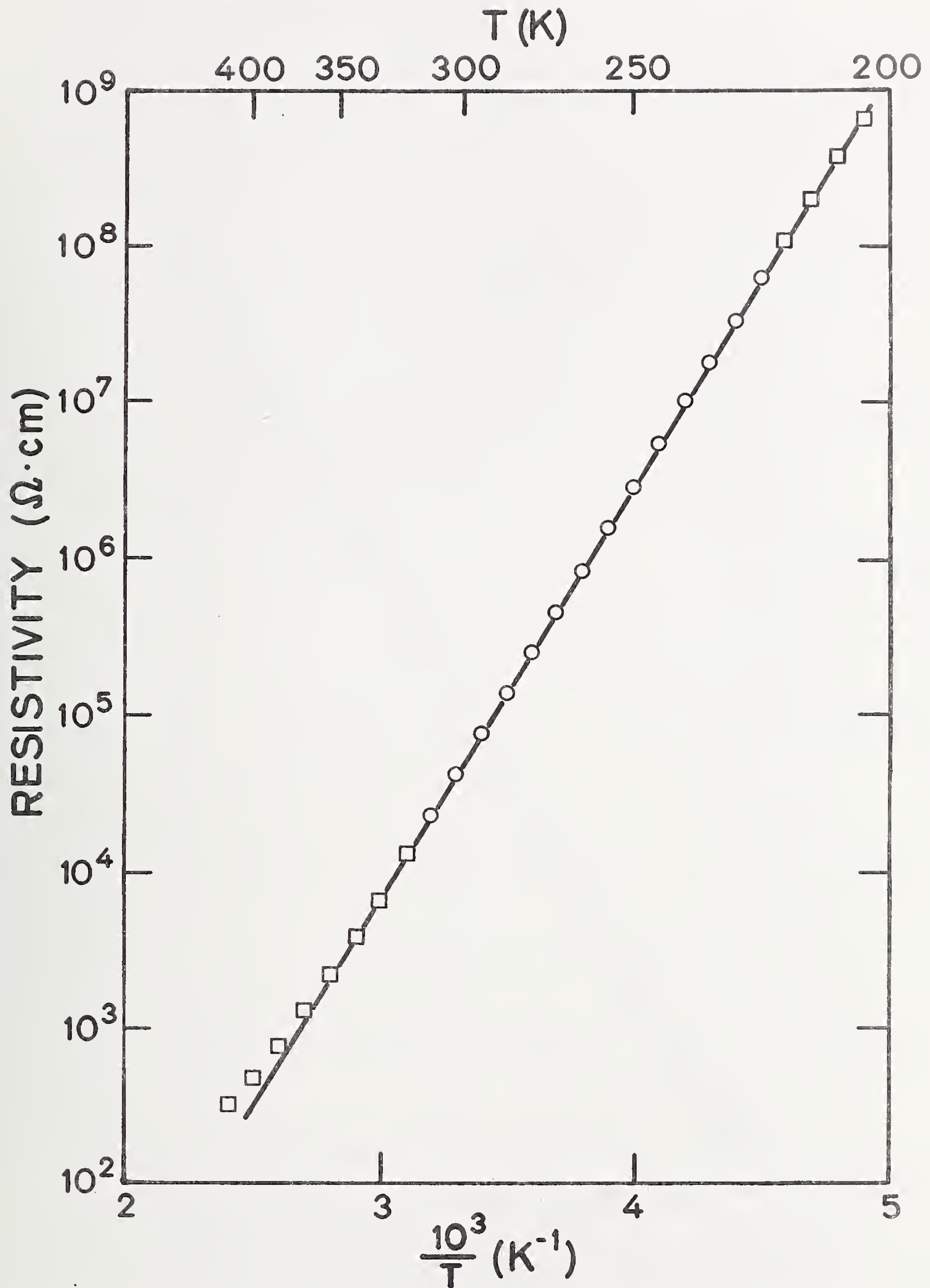

Figure 6. Activation energy plot for the gold acceptor in phosphorus-doped silicon, based on resistivity data.

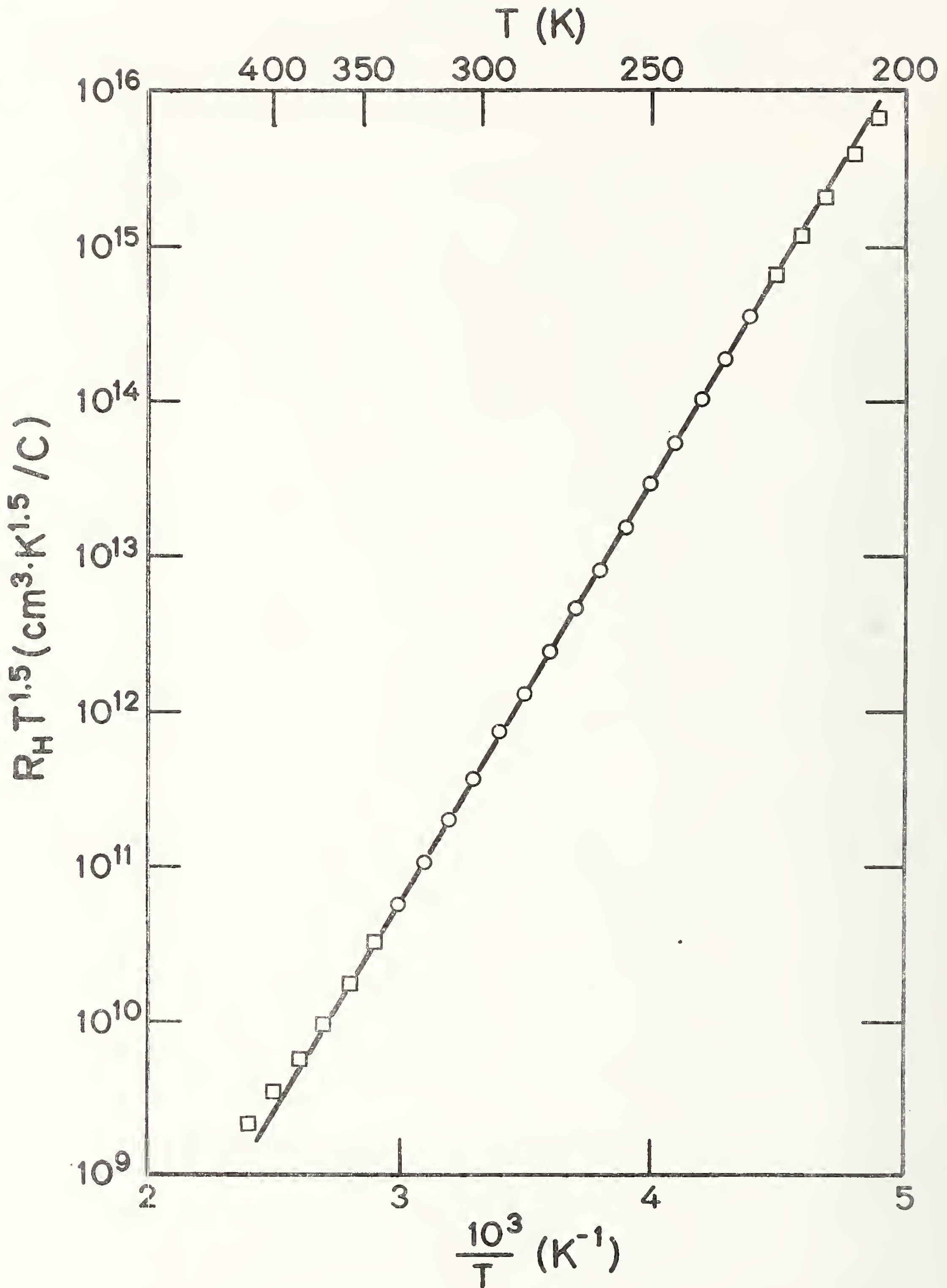

Figure 7. Activation energy plot for the gold acceptor in phosphorus-doped silicon, based on Hall coefficient data.

Table 3 — Experimentally Determined Values of Activation Energies Associated with Gold in Silicon

Level	Specimen Number	Initial Resistivity, $\Omega \cdot cm$	Type	Gold Density, cm^{-3}	Reference Band Edge	Energy, (eV)	
						Resistivity	Hall Effect
Gold Donor	20P950-144	20	*p*	3.9×10^{15}	Valence	0.3469 ± 0.0004	0.3609 ± 0.0003
	20P01250-0.25	20	*p*	3.1×10^{16}	Valence	0.3438 ± 0.0002	0.3620 ± 0.0003
	20P01250-2	20	*p*	9.9×10^{16}	Valence	0.3528 ± 0.0002	0.3613 ± 0.0003
	1100P1250-8	1100	*p*	1.1×10^{17}	Valence	0.3482 ± 0.0004	0.3627 ± 0.0003
Gold Acceptor	80N850-304	75	*n*	3.6×10^{14}	Conduction	0.5247 ± 0.0005	0.5373 ± 0.0003
Shallow Acceptor	1100P1250-8	1100	*p*	*	Valence	0.0349 ± 0.0001	

*Annealed at 600°C for 1 hour in helium

Note — The activation energies determined from resistivity plots show considerable variation from specimen to specimen which may be due to variations in conductivity mobility as the Hall mobilities of these specimens vary in magnitude and temperature dependence. As expected the energies determined from resistivity are smaller than those obtained from Hall effect because of the strong temperature dependence of the mobility as discussed in the text. The experimentally determined values appear to be in reasonable agreement with those chosen for the calculations.

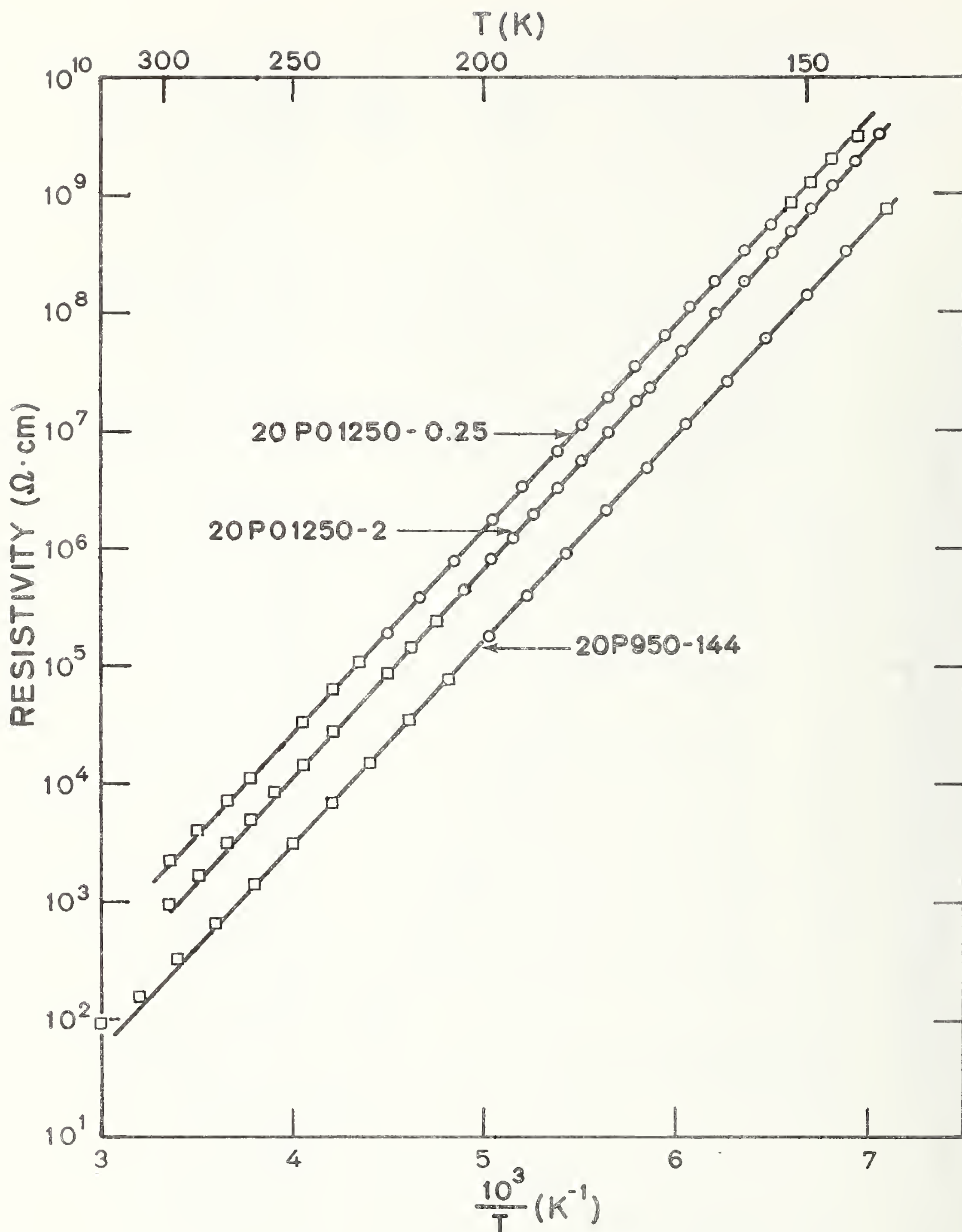

Figure 8. Activation energy plot for the gold donor in boron-doped silicon, based on resistivity data.

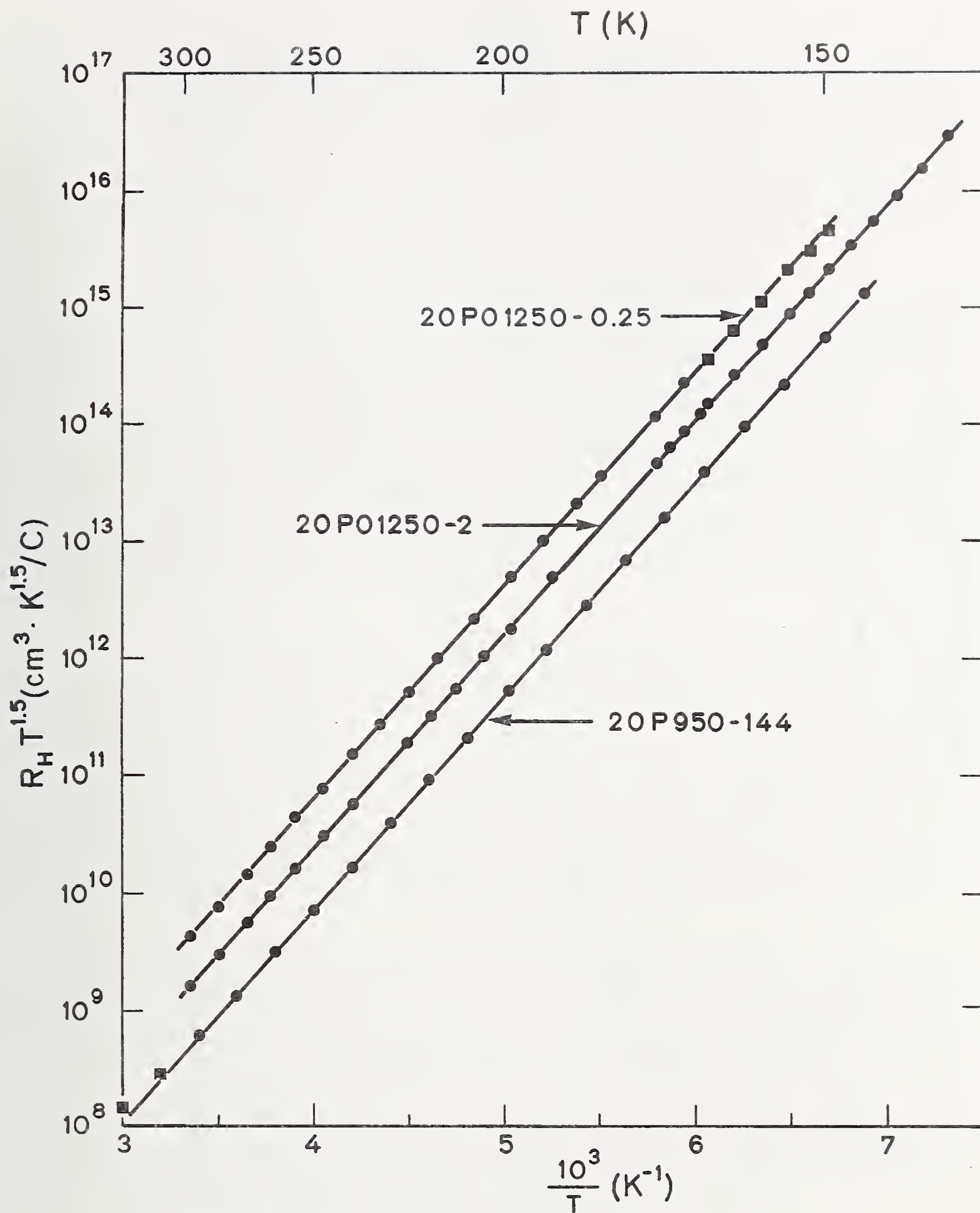

Figure 9. Activation energy plot for the gold donor in boron-doped silicon, based on Hall coefficient data.

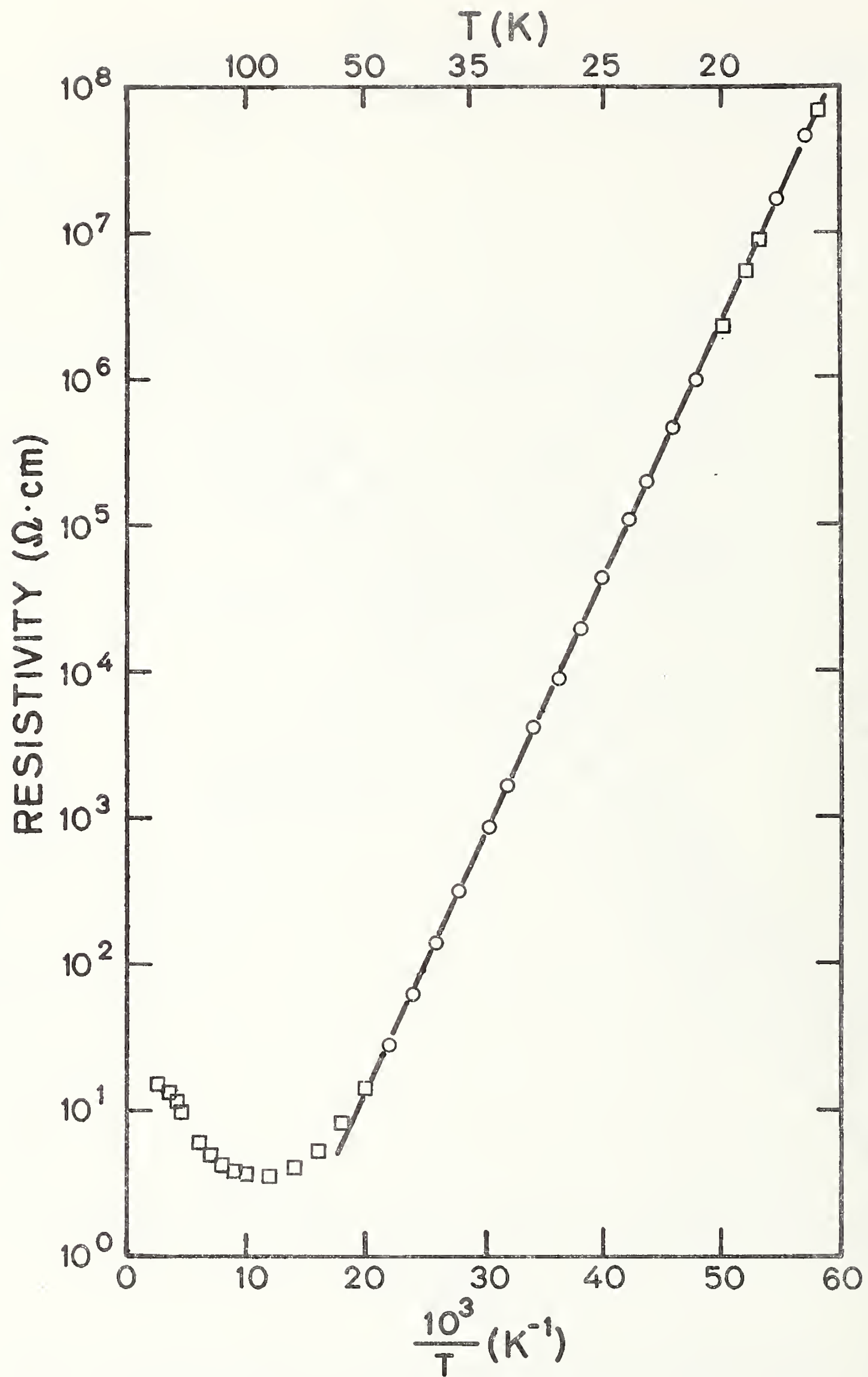

Figure 10. Activation energy plot for the shallow, gold-coupled acceptor in boron-doped silicon, based on resistivity data.

temperature range from 15 to 400 K and are plotted in figure 10 as a function of inverse temperature. An activation energy of 0.0349 ± 0.0001 eV above the valence band edge was calculated from the slope of the linear portion of the curve between 15 and 45 K by the procedure used for the other gold levels. This value is in reasonable agreement with the only other reported value for this level [3]. More observations of this level by a variety of techniques are needed to determine its origin and to obtain a more definite value for its activation energy.

Carrier Mobility — Typical Hall mobilities were calculated from the Hall effect and resistivity data reported above for lightly doped specimens 80N850-304 and 20P950-144, respectively. The electron and hole mobilities, shown in figure 11, are characteristic of lattice scattering and have a $T^{-2.20}$ and $T^{-2.66}$ dependence on temperature, respectively. When corrected for the temperature dependence of the scattering factor, $T^{0.44}$ for electrons and $T^{-0.21}$ for holes [12], the deduced conductivity mobilities have about the same temperature dependence and are in reasonable agreement with direct measurements of the drift mobilities [7]. Additional study and analysis of how the temperature variations of the scattering factors, effective masses, and mobilities depend on doping density are required before quantitative comparisons can be made.

Heat Treatment Studies — Heat treatments were conducted on silicon wafers to study the influence of the high-temperature processing during gold doping on the electrical properties of the specimens. Heat treatments in oxygen and argon atmospheres were carried out at 950°C for 168 h and at 1250°C for 8 h on wafers of float-zoned, *n*- and *p*-type silicon with initial resistivity at room temperature of about 2300 Ω·cm. These treatments were performed in a new quartz tube prior to its use for gold diffusion, with the same heating and quenching procedures used during normal gold diffusions. Portions of each wafer were checked for gold density by activation analysis but none was detected at a sensitivity limit of 7×10^{12} cm^{-3}.

Generally, resistivity and conductivity-type changes in the *p*-type specimens were consistent with the introduction of compensating donors at a density of 10^{12} to 10^{13} cm^{-3}. Greater changes occurred at 1250°C than at 950°C; at the same temperature, more donors were introduced during heat treatments in the argon atmosphere than during those in the oxygen atmosphere. The increased resistivity observed in the *p*-type material suggests that many of the high resistivity data points in figures 1 and 2, which exceed the values predicted by the theoretical curves of resistivity as a function of gold density, could also have been affected by the donors unintentionally introduced during the gold diffusion.

Measurements on the *n*-type specimens generally showed little or no resistivity change after heat treatment. This result suggests that the donors introduced lie well below the phosphorus level and thus do not influence the electrical properties of phosphorus-doped specimens.

The activation energy of the impurity introduced into the initially *p*-type specimen heat treated in an argon atmosphere at 1250°C was found from Hall coefficient data taken in the temperature range 200 to 400 K. After heat treatment, the specimen had converted to *n*-type and had a room temperature resistivity of 3.8×10^4 Ω·cm consistent with the introduction of at

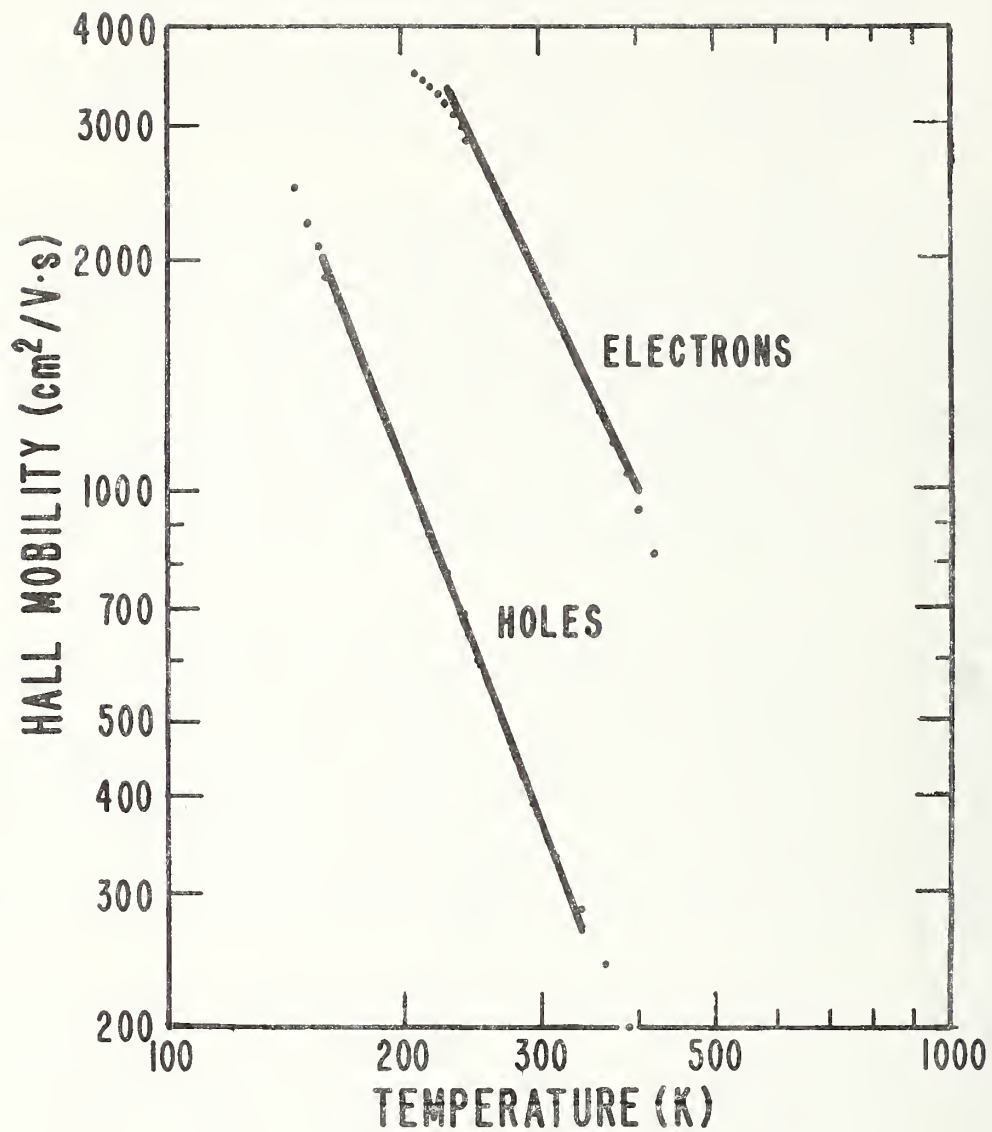

Figure 11. Hall mobility for electrons and for holes in lightly doped silicon as a function of temperature.

least 5×10^{12} donors. The activation energy found, about 0.53 eV, is close to the value of 0.55 eV reported by Collins and Carlson [14] for the upper donor level of iron in silicon. Although there is a similarity with the energy of the gold acceptor, the latter would not result in the observed conversion from *p*- to *n*-type.

Minority carrier lifetime measurements were made by the surface photovoltage method [2] on specimens cut from the wafers in the heat treatment study and compared with lifetime data obtained on untreated wafers cut from the same crystals. The reductions in lifetime following heat treatment ranged from factors of 5 to 500 depending on the specific treatment; at a given time and temperature, heat treatment in argon atmosphere resulted in a lower lifetime than the same treatment in an oxygen atmosphere. Such reductions are consistent with the presence of an efficient recombination center deep in the forbidden gap.

The results reported above suggest that extremely minute amounts of iron, introduced during the preparation of wafers for diffusion, are likely to be responsible for the observed resistivity changes in high resistivity *p*-type silicon.

CARRIER LIFETIME MEASUREMENTS

Surface Photovoltage Method — For reasons discussed previously [2], the steady-state surface photovoltage (SPV) method was studied extensively in connection with application to determining minority carrier lifetime. Determination of lifetime from an SPV measurement requires knowledge of two quantities: the minority carrier diffusion coefficient, which is a function of the impurity concentration in the specimen, and the photon absorption coefficient as a function of wavelength in the region used. Diffusion coefficients have been determined from published data on conductivity and drift mobility [7]. Several sets of absorption coefficient data [2] exist in the literature; these have been used with varying degrees of success.

For silicon which has not been diffused with gold or otherwise heat treated, the absorption coefficient data of Dash and Newman [15], obtained on silicon not stress-relieved, have given the most linear fit to the SPV measurements. Such measurements are normally made on specimens which have been etched to remove a 25-μm thick surface layer. To investigate if a layer of damaged material might be present in an undiffused specimen which required Dash and Newman absorption coefficient data to fit the SPV results, measurements were repeated after a second etch to remove an additional 50-μm thick layer. No significant differences in fit or diffusion length were seen.

For specimens which were diffused to obtain a gold density close to saturation or heat-treated for the same conditions of temperature and time, it was found that the absorption coefficient data of Runyan [16], determined on stress-relieved silicon, gave the best fit to the SPV measurements.

For specimens which were diffused to give a gold density considerably short of saturation, it was found that neither Dash and Newman nor Runyan absorption coefficient data gave a good fit to the SPV measurements. Of other data which were tried, those of Braunstein, *et al.* [17] gave the best fit, but the result was far from satisfactory. There was more than a factor of two variation in the diffusion length obtained from the linear region of the SPV plots made with the various data. To be certain that the SPV measurements were characteristic of the bulk of the specimen, SPV measurements were repeated after etching the specimen to remove a 100-μm thick layer. The results were the same, within experimental error, to those obtained after the etching during initial specimen preparation in which a layer only 25-μm thick was removed. Apparently such a gold diffusion relieves only a portion of the stress which is initially present in the slice, whereas diffusions of sufficient duration to achieve a much larger gold density are adequate to relieve essentially all of the stress in the slice. These experiments also suggest that the property of the crystal which affects the absorption coefficient is characteristic of the bulk material rather than of a surface layer.

To obtain absorption coefficient data appropriate to the heat treatments given the material in this study, optical transmission measurements are underway. The wavelength range used for the SPV measurements in silicon is from about 0.8 to 1.1 μm in the vicinity of the band gap absorption edge. In this range the absorption coefficient changes rapidly from a value of about 1000 cm^{-1} at 0.8 μm to about 10 cm^{-1} at 1.1 μm. A very thin specimen is needed to obtain accurate transmission measurements when the absorption coefficient is high and

thicker ones are required at wavelengths with less absorption. To cover the wavelength range, four chem-mechanically polished silicon wafers were prepared with thicknesses of about 30, 100, 300, and 1000 μm. Measurements have been made on the wafers and they have been heat treated at a temperature and time used for a gold diffusion in preparation for the second set of measurements.

A series of SPV measurements was made on Hall bars cut from boron-doped silicon wafers with gold densitites from 5×10^{14} to 5×10^{15} cm^{-3}. These densities were much less than those of the shallow impurity in the specimens studied. Hence the added gold results in little increase in the resistivity but may give rise to large reductions in the carrier lifetime. The measured diffusion lengths for these specimens ranged from 1 to 10 μm. The lifetime results plotted against gold density showed considerable scatter which could be attributed to a random variation of about ±2 μm in the measured diffusion length. Numerous repetitive measurements on the same specimen confirmed the presence of these random variations. It thus appears that increased control over experimental conditions is necessary to obtain data from which a reliable value of capture cross section can be calculated. Although several improvements in the SPV apparatus and measurement procedures were instituted, it has not yet been possible to reduce the variability to the desired level to permit useful measurements on material with lifetime down to a few nanoseconds.

In a related task area, work was completed on an analysis of SPV measurements in epitaxial layers. The report of this work is included as Appendix C.

Diode Recovery Methods — Because of the difficulties and delays in applying the SPV method to the measurement of short diffusion lengths, attention was redirected toward various diode recovery methods. The work undertaken focused on two test methods which are commonly used to determine minority carrier lifetime: reverse recovery (RR) and open circuit voltage decay (OCVD). The evaluation and development of neither method has been completed; consequently, the following sections cover initial efforts which have been directed toward a better understanding of the methods in preparation for applying them to measurements on gold-doped specimens with short lifetime.

Although both RR and OCVD have gained general acceptance as techniques for determining minority carrier lifetime, there is poor correlation in the minority carrier lifetime computed from the two experiments for the same diode. The results of Bassett and Hogarth [18] and Kao and Davis [19] showed that the minority carrier lifetime, as computed from OCVD and RR experiments and other different experiments, often differed by as much as a factor of 2 to 3. Measurements made in this laboratory on a randomly chosen diode showed that the minority carrier lifetime for this diode as computed from RR and OCVD experiments differed by a factor of roughly 2.5. The thrust of the analytical and experimental work reported in the following sections was to evaluate the RR and OCVD experiments to find out why the lifetimes computed from these experiments often did not agree, and to determine under what circumstances the computed lifetimes could be made to agree.

The devices studied in the RR and OCVD experiments to date have been *p-n* diodes; these devices were selected because of their simplicity. To

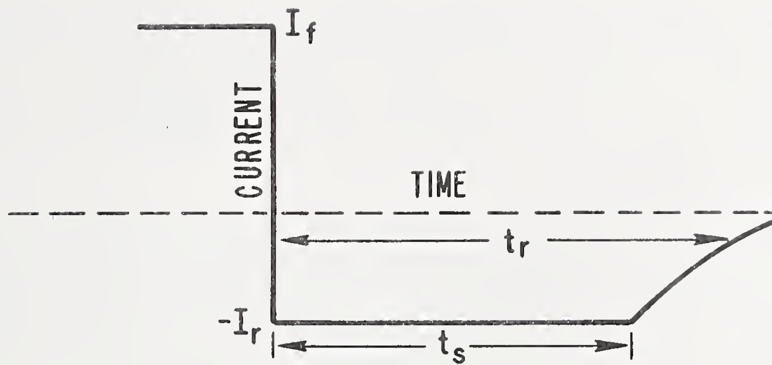

Figure 12. Idealized reverse recovery transient.

make the analysis tractable the following assumptions were made in developing expressions to relate lifetime to the RR and OCVD transients:

1. The *p-n* junction was assumed to be abrupt.

2. The doping level on one side of the junction was assumed to be much greater than the other side so that only minority carriers in the neutral region of the lightly doped side of the junction had to be considered.

3. The device was assumed to have recombination-type contacts so that the excess carrier density at the contacts was zero.

An important variable in the discussion which follows is the width of the neutral region on the lightly doped side of the *p-n* junction; in the literature this is referred to as the diode base width, W. The important parameter in the theory is the ratio of W to the minority carrier diffusion length, L; in the following, a diode whose base width is shorter than 3 to 5 times the diffusion length is called a short base diode.

Reverse Recovery Method — A RR transient is observed whenever a *p-n* junction which has been forward biased for a sufficiently long time is suddenly reverse biased. An idealized wave form is shown in figure 12. Initially the diode is forward biased and conducting a current, I_f; when the bias is abruptly reversed the diode conducts a constant current, I_r, for a time, t_s, called the storage time. At the time t_s after the reversal, the minority carrier density at the interface between the space charge region and the neutral region on the lightly doped side of the junction is equal to the equilibrium minority carrier density in the neutral region. At the same time, it is observed experimentally that the voltage across the

junction is zero. Throughout the recovery phase of the transient which follows, the space charge region depletes, and the current decays to its reverse leakage value. Another time that is referred to in the literature is the recovery time, t_r; this is the time interval between the time the diode is reverse biased to the time required for the reverse current to decay to 10 percent of its initial value.

The possibility of using the reverse recovery transient to determine the lifetime of the minority carriers associated with a device was first investigated by Pell [20]. Kingston [21] used an approximate approach to develop a relation between the ratio of the minority carrier lifetime τ and the storage time and the ratio of the forward and reverse currents for a diode whose base width was infinitely long; he showed that

$$\operatorname{erf} \sqrt{\frac{t_s}{\tau}} = \left[1 + \frac{I_r}{I_f}\right]^{-1} . \tag{9}$$

Lax and Neustadter [22] derived eq (9) rigorously. Byczkowski and Madigan [23] extended Lax and Neustadter's analysis to the case of diodes with arbitrary base width; they showed that

$$\sum_{n=0}^{\infty} \frac{\exp\left\{-[1 + (n + \frac{1}{2})^2(\pi \frac{L}{W})^2] \frac{t_s}{\tau}\right\}}{1 + (n + \frac{1}{2})^2 (\pi \frac{L}{W})^2} = \left[1 + \frac{I_f}{I_r}\right]^{-1} \frac{\frac{W}{L} \tanh \frac{W}{L}}{2} . \tag{10}$$

To investigate the applicability of these relationships, reverse recovery experiments were conducted in two ways:

1. The forward current was fixed at some value, generally 20 mA, and t_s was measured as a function of I_r.

2. Both the forward and reverse currents were varied such the ratio I_f/I_r was constant and t_s was measured as a function of I_r.

The results of the first type of RR experiment showed that the storage times of some diodes varied logarithmically with the forward to reverse current ratio

$$t_s \propto \ln \left(1 + \frac{I_f}{I_r}\right) . \tag{11}$$

Subsequent experiments showed that the data for some diodes could be fitted with eq (11), for example see figure 13, but that data for other diodes could be fitted with eq (9), see figure 14.

Grove and Sah [24] have shown that t_s should vary logarithmically with $(1 + I_f/I_r)$ when $W/L \ll 1$ and $I_f/I_r \gg 1$. This result suggested that t_s varied logarithmically with $(1 + I_f/I_r)$ because the base widths of the diodes were less than or roughly equal to the diffusion length of the minority

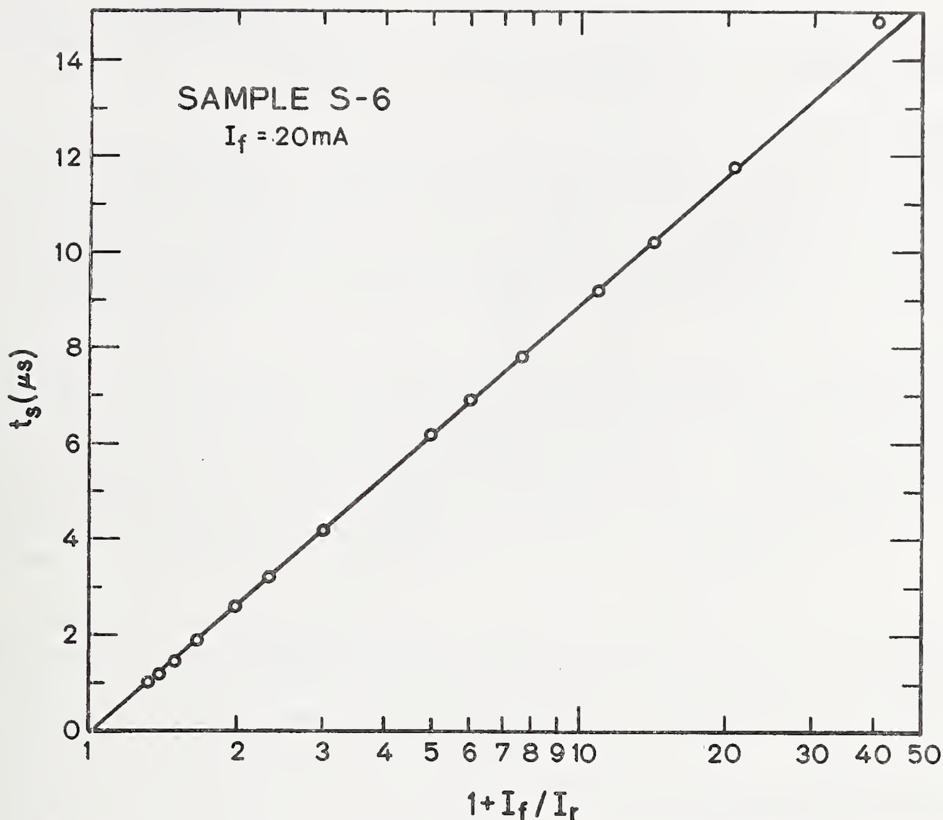

Figure 13. Reverse recovery characteristics of a short base diode. The solid line is calculated from eq (11); experimental points are shown as open circles.

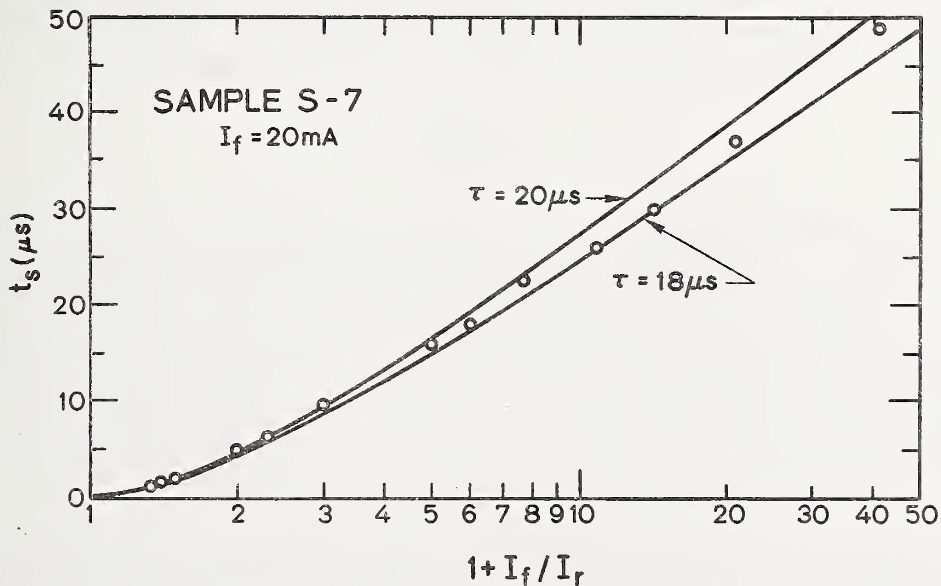

Figure 14. Reverse recovery characteristics of a long base diode. Experimental points are shown as open circles; the solid curves were calculated from eq (9) for two values of τ. For this example, the scatter in the data results in a ±1 μs uncertainty in τ.

carriers. An examination of the dimensions of the diodes which obeyed eq (11) showed they were short base diodes. Also, a check of several diodes which obeyed eq (9) showed that they were long base diodes.

The different functional dependences of t_s on I_f/I_r for a short and long base diodes provides a means to determine whether a particular diode can be characterized as a long or short base diode. If eq (9), with the appropriate choice of τ fits the RR data, the diode can be assumed to be a long base diode; however, if the fit cannot be made and if t_s varies logarithmically with $(1 + I_f/I_r)$, the diode can be considered to be a short base diode.

To study further the effect of diode base width on the RR transient, eq (10) was evaluated for various base widths; the results of these calculations are shown in figure 15. The calculations show that for $W/L > 3$ and $I_f/I_r < 10$, less than 2.5 percent error is introduced in using eq (9) to calculate the minority carrier lifetime rather than eq (10); however, if Lax and Neustadter's expression were used to compute the lifetime in a short base diode ($W/L < 3$), the computed lifetime could be significantly in error.

The results of the second type of RR experiment showed that if I_f and I_r were varied so that the ratio of I_f/I_r was constant, the storage time changed. For five of the eight types of diodes which have been tested, t_s decreased when I_f increased; for the remaining three types of diodes t_s increased. This effect was studied by Owen and Wilkinson [25] who attributed it to saturable traps, but it is not certain at the present time this represents a complete explanation.

Open-Circuit Voltage Decay Method — If a forward biased *p-n* junction is suddenly open circuited, the initial part of the voltage decay transient is often observed to decay linearly with time. An idealized transient is shown in figure 16. Lederhandler and Giacoletto [26] concluded that the slope of the linear part of the voltage decay transient (dV/dt) was related to an effective minority carrier lifetime, τ_e, by the relation

$$\tau_e = -\frac{kT}{q}\left(\frac{dV}{dt}\right)^{-1} \tag{12}$$

where k is Boltzmann's constant, T is absolute temperature, and q is the electronic charge. Subsequent authors have developed and applied his technique to *p-n* and *p-i-n* diodes. Bassett [27] showed that the non-linear variations in the voltage decay which are generally observed at the end of the OCVD transient were due to surface effects. Choo and Mazur [28] developed a general expression for the decay of mobile charge carriers in a *p-n* diode of arbitrary width. From their analysis and experimental results it can be inferred that for short base width, the geometry must be considered in calculating the lifetime for the decay transient.

The results of the OCVD experiments to date indicate that the slope of the linear portion of the OCVD transient is independent of current level. Also, it was noted that when a diode was shunted with a resistor, the duration of the OCVD transient is shortened, but the slope of the linear part of the voltage decay is unaffected. Throughout all of the OCVD experiments a more or less linear voltage decay transient was always observed.

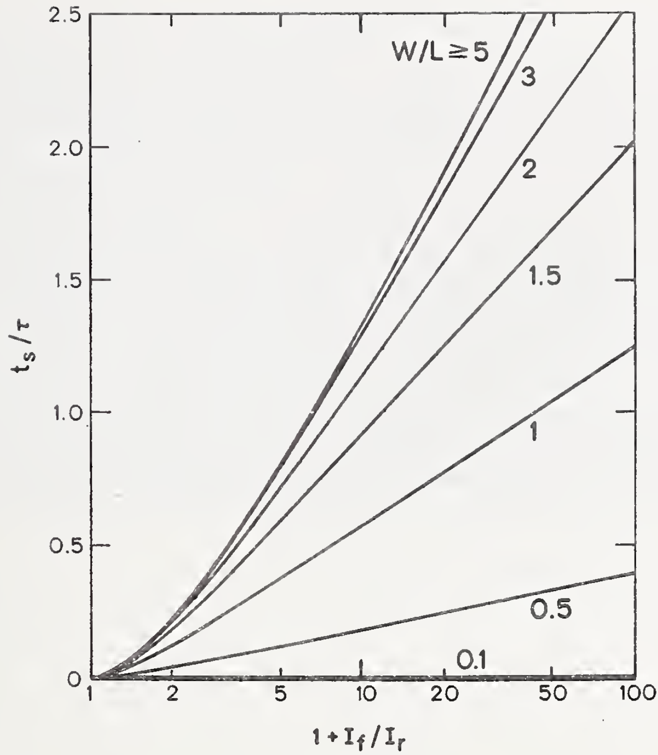

Figure 15. Diode storage time (t_s) normalized to lifetime (τ) as a function of forward-to-reverse current ratio (I_f/I_r) calculated from eq (10). The curve for W/L $\geq$ 5 is identical with eq (9).

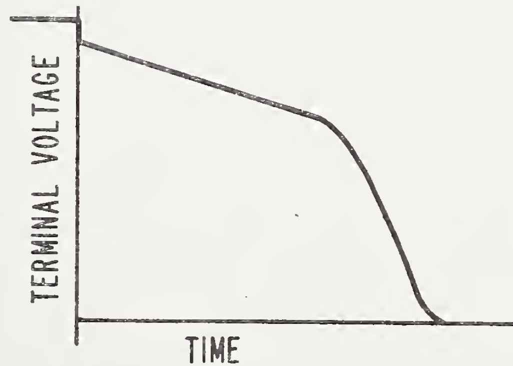

Figure 16. Idealized open circuit voltage decay transient.

Comparisons Between RR and OCVD Measurements — The discussion above has focused on the problems encountered in correlating the lifetime computed from RR and OCVD experiments on short base diodes. The difficulties in correlating the minority carrier lifetimes associated with long base diodes were much less. A comparison of the lifetimes computed from RR and OCVD experiments on diodes for which the RR transient obeyed eq (9) showed that the minority carrier lifetime for a particular device agreed to within ±10 percent of the mean of the two values if a factor of 2 is included on the right-hand side of eq (12) as suggested by Choo and Mazur [28] for high injection in n^+p diodes. RR measurements were made with a forward current of 20 mA. OCVD measurements, which were found not to depend greatly on current level, were generally made with a forward current of 20 mA or more. Since the experimental error in the measurement of I_f, I_r, t_s, and dV/dt was at least ±5 percent, the experimentally determined correlation of ±10 percent was considered to be quite satisfactory. For short base diodes the agreement is not yet this close.

DIRECTIONS FOR FUTURE WORK

More complete characterization of the gold-coupled shallow acceptor and an explanation for the apparent difference between electrically active and total gold densities are required to elucidate the energy level model for gold in silicon.

The next phases of the work involve the study of gold-doped p^+n and n^+p junctions. Fabrication procedures are being developed. These junctions will be used to study, first, the uniformity of gold doping in the vicinity of the junction and, second, the recombination characteristics of the gold centers. The first study will be carried out by using capacitance-voltage and spreading resistance measurements. The second will involve stimulated current and capacitance measurements in addition to RR and OCVD lifetime measurements. Also, these junctions will be useful in studying the dependence of reverse recovery storage time on the magnitude of the current for a constant ratio of I_f to I_r.

REFERENCES

1. Collins, C. B., Carlson, R. O., and Gallagher, C. J., Properties of Gold-Doped Silicon, *Phys. Rev.* 105, 1168-1173 (1957).

2. Thurber, W. R., and Bullis, W. M., Resistivity and Carrier Lifetime in Gold-Doped Silicon, Air Force Cambridge Research Laboratories Report AFCRL-72-0076 (January 31, 1972). Available from National Technical Information Service, Springfield, Virginia 22151, Accession Number AD 740592.

3. Brückner, B., Electrical Properties of Gold-Doped Silicon, *Phys. Status Solidi A* 4, 685-692 (1971).

4. Blakemore, J. S., *Semiconductor Statistics*, pp. 118-120 (Pergamon Press, New York, 1962).

5. Macfarlane, G. G., McLean, T. P., Quarrington, J. E., and Roberts, V., Fine Structure in the Absorption-Edge Spectrum of Si, *Phys. Rev.* 111, 1245-1254 (1958).

6. Barber, H. D., Effective Mass and Intrinsic Concentration in Silicon, *Solid-State Electronics* 10, 1039-1051 (1967).

7. Ludwig, G. W., and Watters, R. L., Drift and Conductivity Mobility in Silicon, *Phys. Rev.* 101, 1699-1701 (1956).

8. Brooks, H., Theory of the Electrical Properties of Germanium and Silicon, *Advances in Electronics and Electron Physics*, Vol. VII, L. Marton, ed., pp. 156-160. (Academic Press, New York, 1955).

9. Bullis, W. M., and Strieter, F. J., Electrical Properties of *n*-Type Silicon Doped with Gold, *J. Appl. Phys.* 39, 314-318 (1968).

10. Schuman, V. B., Diffusion of Gold in Silicon, *Soviet Phys. Semiconductors* 1, 790-791 (1967-68).

11. Brotherton, S. D., and Rogers, T. L., Influence of Dislocations on Gold Diffusion into Thin Silicon Slices, *Solid-State Electronics* 15, 853-860 (1972).

12. Messier, J., and Flores, J. M., Temperature Dependence of Hall Mobility and μ_H/μ_D for Si, *J. Phys. Chem. Solids* 24, 1539-1542 (1963).

13. Natrella, M. G., *Experimental Statistics*, NBS Handbook 91 (August 1, 1963), ¶5-5.1.3.

14. Collins, C. B., and Carlson, R. O., Properties of Silicon Doped with Iron or Copper, *Phys. Rev.* 108, 1409-1414 (1957).

15. Dash, W. C., and Newman, R., Intrinsic Optical Absorption in Single-Crystal Germanium and Silicon at 77°K and 300°K, *Phys. Rev.* 99, 1151-1155 (1955).

16. Runyan, W. R., A Study of the Absorption Coefficient of Silicon in the Wave Length Region between 0.5 and 1.1 Micron, Southern Methodist University Report SMU 83-13 (1967). Available from National Technical Information Service, Springfield, Virginia 22151, Accession Number N68-16510.

17. Braunstein, R., Moore, A. R., and Herman, F., Intrinsic Optical Absorption in Germanium-Silicon Alloys, *Phys. Rev.* 109, 695-710 (1958).

18. Bassett, R. J., and Hogarth, C. A., A Direct Comparison Between Three Different Methods of Measuring the Minority Carrier Lifetime in Thin Silicon Slices, *Int. J. Electronics* 25, 585-590 (1968).

19. Kao, Y. C., and Davis, J. R., Correlations Between Reverse Recovery Time and Lifetime of *p-n* Junction Driven by a Current Ramp, *IEEE Trans. Electron Devices* ED-17, 652-657 (1970).

20. Pell, E. M., Recombination Rate in Germanium by Observation of Pulsed Reverse Characteristic, *Phys. Rev.* 90, 278-279 (1953).

21. Kingston, R. H., Switching Time in Junction Diodes and Junction Transistors, *Proc. IRE* 42, 829-834 (1954).

22. Lax, B., and Neustadter, S. F., Transient Response of a *p-n* Junction, *J. Appl. Phys.* 25, 1148-1154 (1954).

23. Byczkowski, M., and Madigan, J. R., Minority Carrier Lifetime in *p-n* Junction Devices, *J. Appl. Phys.* 28, 878-881 (1957).

24. Grove, A. S., and Sah, C. T., Simple Analytical Approximations to the Switching Times in Narrow Base Diodes, *Solid-State Electronics* 7, 107-110 (1964).

25. Owen, D. B. B., and Wilkinson, E. L. G., Junction Recovery and Trapping in Silicon p^+-n Junctions, *Int. J. Electronics* 20, 21-29 (1966).

26. Lederhandler, S. R., and Giacoletto, L. J., Measurement of Minority Carrier Lifetime and Surface Effects in Junction Devices, *Proc. IRE* 43, 477-483 (1955).

27. Bassett, R. J., Observations on a Method of Determining the Carrier Lifetime in p^+-γ-n^+ Diodes, *Solid-State Electronics* 12, 385-391 (1969).

28. Choo, S. C., and Mazur, R. G., Open Circuit Voltage Decay Behavior of Junction Devices, *Solid-State Electronics* 13, 553-564 (1970).

APPENDIX A

SPECIMEN PREPARATION

Wafers were cut from single crystals of silicon with a diamond saw and lapped to a final thickness of about 1.1 mm with 12-μm alumina. The resistivity of representative wafers was measured by the four-probe [1] or van der Pauw [2] method. To test for radial homogeneity of the shallow doping impurities, the resistivity profile was measured by the four-probe method on one or more wafers from each crystal. After completion of the initial resistivity measurements, both sides of each wafer were chem-mechanically polished [3] in preparation for the gold diffusion.

Immediately prior to insertion in the diffusion furnace, the wafers were cleaned and plated with gold. The cleaning procedure consisted of the following steps: ultrasonic agitation in detergent for one minute, rinses in distilled water and methanol, ultrasonic agitation in trichloroethylene for one minute, rinse in methanol, ultrasonic agitation in methanol, soaking in chromic acid for at least one minute, rinses in distilled water and methanol, three rinses in nitric acid of one minute each, rinses in distilled water and methanol, soaking in hydrofluoric acid for one minute, and final rinses in distilled water and methanol. A 40-nm thick layer of gold was then evaporated on both sides of the wafer and the wafer was loaded into the quartz tube of the diffusion furnace.

Diffusion took place in an open-tube system. Most of the diffusions were done in an atmosphere of high-purity oxygen, which flowed through the quartz diffusion tube at a rate of 4×10^{-6} m^3/s. Diffusions were generally made at temperatures of 850, 950, 1050, 1150, and 1250°C, although other temperatures were also used when more closely spaced values of gold density were desired. Diffusion times varied from 2 weeks at 850°C to 8 hours at 1250°C. The wafers were quenched by pulling them to the cool end of the diffusion tube and then placing them on an aluminum block.

To estimate the uniformity of the gold as a function of depth, spreading resistance measurements were made on portions of a gold-diffused wafer. The starting material was 1.1-Ω·cm, boron-doped silicon; a companion wafer diffused at the same time had a final resistivity of 2.1 Ω·cm and a gold density of 5.1×10^{15} cm^{-3}. A portion of the wafer was lapped at an angle of 5 deg 43 min to study the uniformity through more than half the wafer thickness and another portion was lapped at an angle of 1 deg 9 min to obtain more resolution in the region close to the wafer surface. Two-probe spreading resistance measurements were made on the angle-lapped portions by an apparatus which automatically stepped the probes and recorded the data. The resulting plots showed that the resistance was constant in the center region and that the expected increase in resistance due to excess gold occurred only within 15 to 20 μm from the wafer surface. To eliminate gold in the surface regions, each side of the wafer was lapped to remove a 125-μm thick layer before any measurements were made.

Hall bars with four side arms and expanded ends designed to meet the specifications of the standard method for Hall effect measurements [2] were cut ultrasonically from the lapped wafers for electrical measurements.

Aluminum contact pads were evaporated on one surface of the side arms and ends. Pressure contact to the aluminum pads was made with flat phosphor-bronze springs and the measurements were made in a light-tight holder. Some early data were obtained at room-temperature (25 ± 1°C) equilibrium whereas more recent measurements have been made with the temperature maintained at 24.8 ± 0.1°C by a temperature control system. The latter method has proved superior in that drifts in the resistivity with time are no longer present.

REFERENCES

1. Standard Method for Measuring Resistivity of Silicon Slices with a Collinear Four-Probe Array (ASTM Designation: F84-72), *Annual Book of ASTM Standards*, Part 8 (American Society for Testing and Materials, Philadelphia, 1972).

2. Standard Method for Measuring Hall Mobility in Extrinsic Semiconductor Single Crystals (ASTM Designation: F76-72), *Annual Book of ASTM Standards*, Part 8 (American Society for Testing and Materials, Philadelphia, 1972).

3. Buehler, M. G., Peripheral and Diffused Layer Effects on Doping Profiles, *IEEE Trans. Electron Devices*, ED-19, 1171-1178 (1972). (Patent)

APPENDIX B

ACTIVATION ANALYSIS

For the analysis of gold density a disc was cut ultrasonically from the remainder of the wafer. The density was determined by neutron activation analysis using the following procedure. The silicon specimens and standard were encapsulated in polyethylene vials and irradiated for either 30 or 60 min at a neutron flux of 1 to 6×10^{13} $cm^{-2} \cdot s^{-1}$. Copper foils were attached to each specimen and to the standard to normalize for flux variation. The standard consisted of a filter paper approximately the shape and size of the silicon specimens on which was pipetted a known solution of gold in aqua regia. After irradiation the specimens were allowed to decay for two to four days to minimize short-lived interferences and then counted using a lithium-drifted germanium gamma-ray detector in conjunction with a multi-channel analyzer. The results were calculated using the standard-comparator method.

Solid-State Electronics, 1972, Vol. 15, pp. 1097–1102. Pergamon Press. Printed in Great Britain

INTERPRETATION OF STEADY-STATE SURFACE PHOTOVOLTAGE MEASUREMENTS IN EPITAXIAL SEMICONDUCTOR LAYERS

W. E. PHILLIPS
Institute for Applied Technology, National Bureau of Standards, Washington, D.C. 20234, U.S.A.

(*Received* 24 *January* 1972; *in revised form* 12 *April* 1972)

Abstract—Analysis of the steady-state surface photovoltage (SPV) method of measuring minority carrier diffusion length (L) has been extended to the case of an epitaxial layer on a thick substrate. In layers with thickness greater than four diffusion lengths, the measurement yields the bulk value of L. For layers thinner than $0.5L$, the measured value is that of the substrate. For intermediate thicknesses, the bulk value of L can be estimated. The method also provides a sensitive means of observing the influence of surface conditions on the absorption characteristics of silicon.

NOTATION

A, B, C	boundary condition constants (m^{-3})
A_0, B_0	functions defined by equations 10 and 11
d	thickness of epitaxial layer (m)
D	minority carrier diffusion coefficient (m^2/sec)
I_0	photon intensity at front surface of specimen ($sec^{-1}m^{-2}$)
k	Boltzmann's constant (J °K^{-1})
L	bulk diffusion length (m)
L_0	effective diffusion length or SPV intercept value (m)
$p(x)$	excess minority carrier density at x (m^{-3})
p_0	equilibrium minority carrier density in the substrate (m^{-3})
q	electronic charge (C)
Q	function defined by equation (8)
R	reflectance of the front surface
R_0	ratio defined by equation (12)
s	surface recombination velocity at front surface of specimen (m/sec)
T	temperature (°K)
V	bias voltage across junction (V)
V_{SPV}	amplitude of the SPV signal (V)
x	distance measured from front surface under native oxide (m)
x_0	value of α^{-1} at which Taylor expansion is made (m)
α	absorption coefficient (m^{-1})
γ	quantum efficiency (carrier pair/quantum)
ϕ	built-in (self-diffusion) junction potential (V)
τ	bulk minority carrier lifetime (sec)
Subscript 1	refers to front region (epitaxial layer)
Subscript 2	refers to substrate region

THE INCREASING use and sophistication of devices made of epitaxial semiconductor materials has increased the need for characterization parameters for such materials. The steady-state surface photovoltage (SPV) method is capable of measuring bulk minority carrier diffusion lengths under the surface and by a suitable choice of wavelengths the measurement can be confined to thin regions such as epitaxial layers. The measurement is also independent of surface conditions; however, as is discussed below, the type of surface must be considered in the choice of appropriate absorption coefficients.

Analysis of the SPV method has been extended to the case of an extrinsic epitaxial layer on a thick substrate of the same conductivity type with an equal or shorter diffusion length. It appears that the SPV method is suitable for measuring diffusion length or carrier lifetime in the epitaxial layer for material in which the diffusion length is less than about a quarter of the thickness of the epitaxial layer. For epitaxial material in which the effective diffusion length, L_0, is greater than twice the epitaxial layer thickness, the method measures substrate diffusion length. For epitaxial thicknesses in the range between $0.5\,L_0$ and $4L_0$, a knowledge of the substrate diffusion length, impurity concentrations, and epitaxial layer thickness permits a determination of the diffusion length in the epitaxial layer.

SPV measurements in thick specimens have been analyzed by Goodman[1] and by Bergmann, Fritzsche, and Riccius[2] with the assumptions that the diffusion length and the reciprocal absorption coefficient are much less than the specimen

thickness and much greater than the depth of the surface space-charge region. The material is assumed to be extrinsic and the excess carrier density small compared to the majority carrier thermal equilibrium density. Trapping was neglected. Under these conditions, the surface photovoltage is a function of the excess minority charge density injected into the surface space-charge layer. If small variations in quantum efficiency and reflectance with wavelength are neglected, the incident light intensity, I_0, required to produce a given SPV, V_{SPV}, is a linear function of reciprocal absorption coefficient, α^{-1}:

$$I_0 = \text{constant}\ (\alpha^{-1} + L). \qquad (1)$$

The plot of I_0 against α^{-1} has an extrapolated intercept for $I_0 = 0$ at $\alpha^{-1} = -L$.

For thin layers such as epitaxial layers, the condition that the diffusion length be much less than the thickness may not be met. However, even when the condition was not met, experimental SPV plots of I_0 against α^{-1} still were found to yield a straight line. The present analysis was undertaken in order to investigate this experimental result.

A mathematical model was developed by adding a region to represent the epitaxial layer, which may be thin, in front of a region to represent the substrate, assumed to be thick compared to the diffusion length. Trapping effects were again omitted since Choo and Sanderson[3] have shown that majority trapping and moderate minority trapping do not influence the SPV measurement at the low injection levels which are appropriate for the method.

The steady-state current continuity equation was solved to obtain the excess minority carrier density in both regions, $p_1(x)$ and $p_2(x)$. Under the conditions for which a one-dimensional analysis is valid and for small electric fields, the solution in the epitaxial layer is:*

$$p_1(x) = A\mathrm{e}^{-x/L_1} + B\mathrm{e}^{x/L_1} + \frac{\gamma I_0(1-R)\alpha\tau_1\mathrm{e}^{-\alpha x}}{1-(\alpha L_1)^2} \qquad (2)$$

and the solution in the thick substrate is:*

$$p_2(x) = C\mathrm{e}^{-(x-d)/L_2} + \frac{\gamma I_0(1-R)\alpha\tau_2\mathrm{e}^{-\alpha x}}{1-(\alpha L_2)^2}. \qquad (3)$$

The constants A, B, and C are evaluated from the front surface recombination velocity of the epitaxial layer, the continuity of current across the epitaxial-substrate junction, and the potential difference across the junction.

At the front surface, $x = 0$,

$$D_1\, \mathrm{d}p_1/\mathrm{d}x = sp_1. \qquad (4)$$

The continuity of minority carrier current across the epitaxial–substrate junction yields the equation at $x = d$:

$$\frac{\mathrm{d}p_1}{\mathrm{d}x} = \frac{D_2}{D_1}\frac{\mathrm{d}p_2}{\mathrm{d}x}. \qquad (5)$$

Generalized boundary conditions for semiconductor junctions have been derived by Harrick [5] and Fletcher[6]. For heavily doped substrates of the same conductivity type (n on n^+ or p on p^+), their equations simplify to the condition:

$$p_2(d) = p_1(d)\mathrm{e}^{-(q\phi/kT)} + p_0 qV/kT. \qquad (6)$$

Because the signal is extracted through a capacitance, the bias voltage, V, is essentially zero. With $V = 0$ and a highly doped substrate, the Fermi level

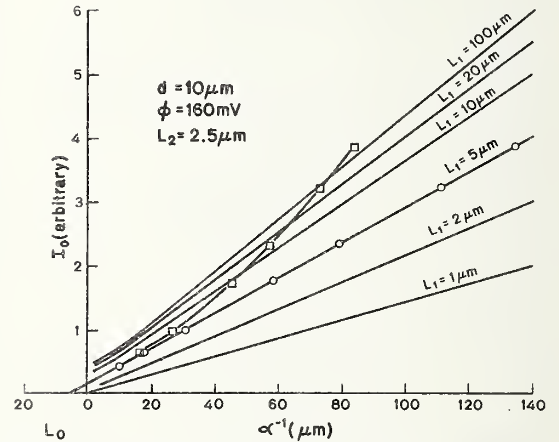

Fig. 1. Theoretical photon intensity required to produce a given SPV response as a function of reciprocal absorption coefficients for various diffusion lengths and a specimen thickness of 10 μm. See text for meaning of data points.

*Sawyer and Rediker[4] showed that this type function remains well behaved at αL_1 (or αL_2) = 1. The solution then is the same except that the last term becomes $0.5\,\gamma I_0(1-R)\alpha^2 x\tau\mathrm{e}^{-\alpha x}$.

is near the band edge in both the substrate and the junction region so that recombination in the space-charge region need not be distinguished from substrate recombination.

Subject to the boundary conditions of equations (4)–(6), and the previously assumed conditions[2], except for the relaxation of the thickness condition $d \gg L$, the constants A, B, and C can be tediously but straightforwardly evaluated for a constant $p_0(0)$ which corresponds to a given V_{SPV}. The resultant equation is then solved for the photon intensity required to produce the given V_{SPV} as:

$$I_0 = \frac{p_1(0)}{\gamma(1-R)\tau_1}\left(\frac{1-\alpha^2L_1^2}{\alpha}\right)Q \div \left\{\sinh\frac{d}{L_1} - \alpha L_1 \cosh\frac{d}{L_1} + \frac{D_2L_1}{D_1L_2}e^{-q\phi/kT}\left(\cosh\frac{d}{L_1} - \alpha L_1 \sinh\frac{d}{L_1}\right) + 2e^{-\alpha d}\left[\alpha L_1 - \frac{D_2L_1}{D_1L_2}e^{-q\phi/kT} + \left(\frac{L_1}{L_2} - \alpha L_1\right)\left(\frac{\frac{1}{(\alpha L_1)^2} - 1}{\frac{1}{(\alpha L_2)^2} - 1}\right)\right]\right\}, \tag{7}$$

where

$$Q = \sinh\frac{d}{L_1} + \frac{sL_1}{D_1}\cosh\frac{d}{L_1} + \frac{D_2L_1}{D_1L_2}e^{-q\phi/kT} \times \left(\cosh\frac{d}{L_1} + \frac{sL_1}{D_1}\sinh\frac{d}{L_1}\right). \tag{8}$$

A plot of I_0 (in arbitrary units)* against α^{-1} is shown in Fig. 1 for various epitaxial layer diffusion lengths and for an epitaxial layer thickness of 10 μm, a substrate diffusion length of 2.5 μm, and a built-in junction potential of 160 mV which would be expected for the material described in the next paragraph. The relationship is seen to be nearly linear.

The experimental values of intensity shown in Fig. 1 were measured by the procedure given in the Appendix and are for a 5 Ω cm *n*-type silicon layer 10 μm thick on a 0.0095 Ω cm antimony-doped (111) substrate 250 μm thick. Those experimental values of intensity identified by circles are plotted against the reciprocal absorption coefficients of Runyan[7] and the same values identified by squares are plotted against the reciprocal absorption coefficients of Dash and Newman[8]. When Runyan's coefficients are used, the experimental points produce a straight line in agreement with the theory. When the points are plotted against the coefficients of Dash and Newman, a straight line is not obtained.

The difference in absorption coefficients may be due to surface stresses in the silicon single crystals used by Dash and Newman. The Runyan coefficients were determined in stress-relieved epitaxial silicon. To test this hypothesis, SPV data from a single crystal specimen with a lapped surface were plotted against both sets of coefficients. The linear plot was that against Dash and Newman coefficients. The surface of the specimen was polished with a cupric ion chemical–mechanical treatment[9] and the SPV data were retaken and the plots redone. The linear plot was then obtained for the Runyan coefficients. The intercept values of both linear plots were in good agreement. From this it was concluded that the Runyan coefficients are appropriate for the experimental data in Fig. 1.

The linearity of the theoretical SPV plot was further investigated by making a Taylor series expansion of I_0 about the point $\alpha^{-1} = x_0$. The intercept, L_0, was calculated as:

$$L_0 = (x_0^2 - L_1^2)(A_0/B_0) - x_0 \tag{9}$$

where

$$A_0 = x_0 \sinh\frac{d}{L_1} - L_1\cosh\frac{d}{L_1} + \frac{D_2L_1}{D_1L_2}e^{-q\phi/kT} \times \left(x_0\cosh\frac{d}{L_1} - L_1\sinh\frac{d}{L_1}\right) + 2L_1R_0e^{-d/x_0} \tag{10}$$

$$B_0 = 2x_0\left[x_0\sinh\frac{d}{L_1} - L_1\cosh\frac{d}{L_1} + \frac{D_2L_1}{D_1L_2}e^{-q\phi/kT} \times \left(x_0\cosh\frac{d}{L_1} - L_1\sinh\frac{d}{L_1}\right)\right] + 4x_0L_1R_0e^{-d/x_0} - (x_0^2 - L_1^2)\left(\sinh\frac{d}{L_1} + \frac{D_2L_1}{D_1L_2}e^{-q\phi/kT}\cosh\frac{d}{L_1}\right) - \frac{2dL_1R_0(x_0^2 - L_1^2)}{x_0^2}e^{-d/x_0} - 2(x_0^2 - L_1^2)e^{-d/x_0}$$

*At short diffusion lengths the variation with wavelength in the term $(1-R)$ becomes important so that the quantity actually plotted is $I_0(1-R)$ as described in the Appendix. Without the correction L_0 would be 5.2 μm instead of 5.0 μm.

$$\times\left[\frac{L_1}{L_2}\left(\frac{\left(\frac{x_0}{L_1}\right)^2-1}{\left(\frac{x_0}{L_2}\right)^2-1}\right)-\frac{D_2L_1}{D_1L_2}e^{-q\phi/kT}\right.$$

$$\left.+\frac{2x_0\left(\frac{L_1x_0}{L_2}-L_1\right)\left(\frac{1}{L_2^2}-\frac{1}{L_1^2}\right)}{\left[\left(\frac{x_0}{L_2}\right)^2-1\right]^2}\right] \qquad (11)$$

and

$$R_0=1-\frac{D_2x_0}{D_1L_2}e^{-q\phi/kT}+\left(\frac{x_0}{L_2}-1\right)\left(\frac{\left(\frac{x_0}{L_1}\right)^2-1}{\left(\frac{x_0}{L_2}\right)^2-1}\right). \qquad (12)$$

A plot of the diffusion length in the epitaxial layer normalized to the intercept value, L_0, against the epitaxial layer thickness, d, also normalized to units of the intercept value, is shown in Fig. 2 for various ratios of epitaxial layer to substrate diffusion lengths, L_1/L_2, and for $d = 10\ \mu$m and $x_0 = 150\ \mu$m. The same quantities are shown in Fig. 3 for various ratios of L_2/d. Other values of $x_0 > 20\ \mu$m give the same results. For values of $L_2 > d$, values of $L_1 < L_2$ are not plotted since they violate the boundary conditions assumed.

It can be seen from both Figs. 2 and 3 that for specimens of thickness greater than about four diffusion lengths, the effective diffusion length, L_0, as given by the (negative) intercept is the bulk diffusion length (i.e., $L_1/L_0 = 1$). This conclusion is in agreement with the results for thick specimens

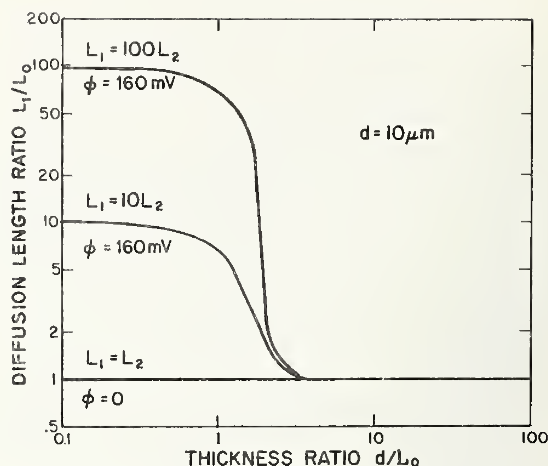

Fig. 2. Calculated SPV minority carrier diffusion length in an epitaxial layer as a function of layer thickness, both normalized to SPV intercept length, for various fixed ratios of L_1 to L_2.

previously reported[1, 2]. For thin epitaxial layers with $d/L_0 < 0.5$, the intercept value is independent of the epitaxial layer bulk diffusion length L_1, but is the diffusion length of the substrate. Intermediate values of d/L_0 lie in a transition region.

For the interpretation of values of L_0 in the transition region, $0.5L_0 < d < 4L_0$, a plot like Fig. 3 with appropriate values of L_2 and ϕ is useful. Higher junction potentials, ϕ, converge the curves for $d/L_2 > 2$ upon the $d/L_0 = 2$ coordinate. The diffusion length ratio corresponding to the appropriate value of d/L_0 is the multiplicative correction factor to convert the effective diffusion length to

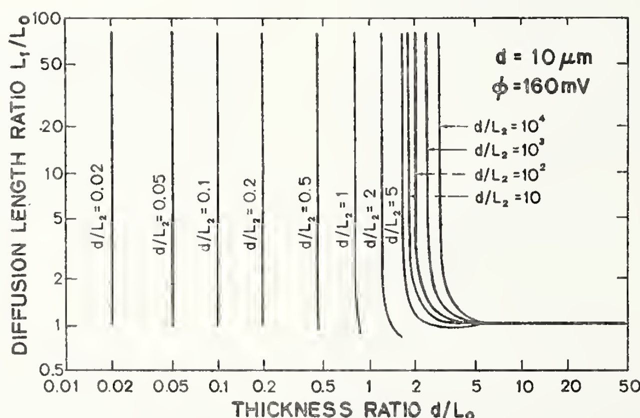

Fig. 3. Same as Fig. 2 except for various fixed ratios of d to L_2.

the bulk diffusion length. For example, the experimental measurement shown in Fig. 1 indicates an L_0 of about 5 μm. An SPV measurement on the back surface of the specimen yielded a value of 2.5 μm for L_2. Since $d/L_0 = 2$ and $d/L_2 = 4$, Fig. 3 can be interpolated to give a value of L_1/L_0 very nearly unity so that $L_1 = L_0 = 5$ μm. This value confirms the theoretical result shown in Fig. 1.

The independence of L_0 on L_1 when $d/L_0 < 0.5$ can be explained by considering the interface to be an imperfectly reflective boundary so that the image of the front surface acts as a carrier sink which limits the effective diffusion length under such conditions. However, in the SPV method, the excess minority carrier density at the front surface is kept constant so that the surface recombination should not play a role in the measurement. This behavior is supported by the fact that the surface recombination velocity s cancels for all values of s in equation (9) and appears in equation (7) only in Q which affects the arbitrary amplitude of the SPV plot. Since the surface recombination is held constant, then one is able to see the effects of carrier leakage through the interface which is dependent upon the substrate diffusion length. However, the surface recombination velocity can be varied to improve sensitivity through the amplitude dependency. The analysis indicates that the optimum value for s is near D_1/L_1.

Demands upon the precision of the measurements increase for shorter diffusion lengths. The precision can be improved by making additional measurements at intermediate wavelengths.

It can be concluded from this work that the SPV method is suitable for measuring effective carrier diffusion lengths. When the epitaxial layer is four or more diffusion lengths in thickness, the measured value is the bulk diffusion length of the epitaxial material. When the epitaxial layer is thinner than about four diffusion lengths, the measured value of diffusion length is an effective value which also depends upon the substrate diffusion length.

This limitation on diffusion length measurements in thin layers was also found by Byczkowski and Madigan[10] on measuring carrier lifetime in p–n junction devices by the reverse recovery method. They found that for base width greater than three diffusion lengths, the recovery time is proportional to the carrier lifetime; but for base widths less than one diffusion length, the ratio of recovery time to carrier lifetime is proportional to the square of the ratio of the base width to diffusion length. This can be restated as the recovery time is proportional to the base transit time. Grove and Sah[11] have also pointed out that the switching process in a narrow base diode is entirely independent of carrier lifetime. P. Chaput and co-workers [12] found that a minimum thickness of 2.5 diffusion lengths is needed to measure minority carrier lifetime in 500 Ω cm silicon with the photomagnetoelectric effect.

It can be generalized from this work and from the works cited that diffusion length type measurements are inadequate characterization parameters for bulk properties of semiconductor materials within a few diffusion lengths of a carrier source or sink. However, when the effective diffusion length is in the transition range of $d/4$ to $2d$, the bulk diffusion length can be estimated from SPV measurements. It is fortunate that under the conditions which yield an effective diffusion length rather than a bulk diffusion length measurement, the effective value is often more useful.

It was also shown that the absorption characteristics of silicon are influenced by surface conditions and that the SPV method provides a sensitive means of observing differences in surface conditions.

Acknowledgements—Measurements were made on epitaxial silicon wafers supplied through the generosity of Dr. F. L. Gittler and Bell Telephone Laboratories, Allentown, Pennsylvania. Appreciation is expressed to Mr. A. W. Stallings for his ingenious fabrication of the equipment and for his care in making measurements and to Mr. D. E. Sawyer for insights in the interpretation of both theory and experimental results. The contributions of Dr. W. M. Bullis to all aspects to this work are also gratefully acknowledged.

REFERENCES

1. A. M. Goodman, *J. appl. Phys.* **32**, 2550 (1961).
2. F. Bergmann, C. Fritzsche and H. D. Riccius, *Telefunken Ztg.* **37**, 186 (1964).
3. S. C. Choo and A. C. Sanderson, *Solid-St. Electron.* **13**, 609 (1970).
4. D. E. Sawyer and R. H. Rediker, *Proc. Instn. Radio Engrs.* **46**, 1122 (1958).
5. N. J. Harrick, *J. appl. Phys.* **29**, 764 (1958).
6. N. H. Fletcher, *J. Electron.* **2**, 609 (1957).
7. W. R. Runyan, Southern Methodist University Report SMU 83-13 (1967). Also NASA CR 93154; and available from National Technical Information Service as N68-16510.
8. W. C. Dash and R. Newman, *Phys. Rev.* **99**, 1151 (1955).
9. E. Mendel and K. H. Yang, *Proc. IEEE* **57**, 1476 (1969).

10. M. Byczkowski and J. R. Madigan, *J. appl. Phys.* **28**, 878 (1957).
11. A. S. Grove and C. T. Sah, *Solid-St. Electron.* **7**, 107 (1964).
12. P. Chaput, D. Blanc, E. Casanovas, A. Peyre-Lavigne, A.-M. Chapuis and S. Soudain, *Electronics Lett.* **2**, 223 (1966).
13. H. R. Philipp and E. A. Taft, *Phys. Rev.* **120**, 37 (1960).

APPENDIX

The experimental SPV data reported in this paper were obtained by the following procedure. The epitaxial surface of the specimen was illuminated with a mechanically chopped output of a monochromator at successive wavelengths of 0.80, 0.85, 0.90, 0.95, 0.97, 0.99, and 1.00 μm. The surface photovoltage signal was capacitively coupled into a phase-sensitive lock-in amplifier synchronized with the mechanical chopper. The monochromator intensity was adjusted at each wavelength to produce a SPV signal of 250 μV. A portion of the illumination was applied through an equivalent optical path to a thermopile detector whose output was detected with a lock-in amplifier. To obtain a number proportional to the photon intensity, I_0, the output reading was multiplied by the wavelength and by a term that corrects for the slight wavelength dependence of the reflectivity at the front surface of the specimen. This term $(1-R)$ is computed from a mathematical representation, valid for $0.7 < \lambda < 1.05\ \mu$m, of the data of Philipp and Taft[13]:

$$1-R = 0.6786+0.03565\lambda^{-1}-0.03149\lambda^{-2}.$$

These values of I_0 were plotted against the reciprocal absorption coefficients for the corresponding wavelengths and a straight line was fitted to the points. A programmable desk calculator with a typewriter output was used to process, plot, store and print out the data. A typical print out is shown in Fig. 4. The specimen is the same as in Fig. 1.

The appropriate reciprocal absorption coefficients are calculated from a mathematical representation of the data of Runyan[7] (for stress-relieved silicon) as:

$$\alpha^{-1} = [0.526367-1.14425\lambda^{-1}+0.585368\lambda^{-2}+0.039958\lambda^{-3}]^{-1}$$

or the data of Dash and Newman[8] (for lapped surfaces) as:

$$\alpha^{-1} = [-1.06964+3.34982\lambda^{-1}-3.61649\lambda^{-2}+1.34831\lambda^{-3}]^{-1}.$$

The calculation of the intercept, L_0, and the computed one sigma standard deviation, s_{b0}, is as follows:

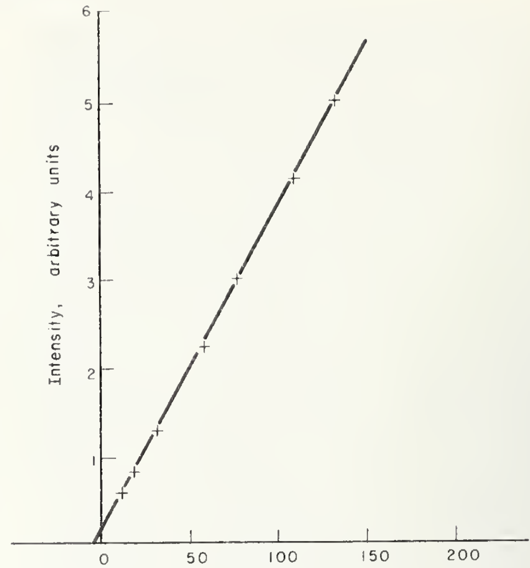

L_0, μm $\qquad$ α^{-1}, μm

WAVELENGTH	T C VOLTACE	RECIPR ABS COEFFI	INTENSITY
1.000 µm	12.00 µV	134.306 µm	8.193
.990	10.00	111.159	6.756
.970	7.40	79.063	4.894
.950	5.65	58.450	3.656
.900	3.45	30.797	2.109
.850	2.35	18.032	1.352
.800	1.80	11.269	.970

Lo = 4.9618 µm SIGMA = .4612 µm SPECIMEN: EPI 3

SPV SIGNAL = 250 µV

Fig. 4. A programmable desk calculator plot and printout of a typical SPV measurement.

$$L_0 = (\Sigma I_0 S_{xx}/S_{xy} - \Sigma\alpha^{-1})/N$$

$$s_{b0} = \left[\frac{S_{xx}-S_{xy}^2/S_{yy}}{N-2}\left(\frac{1}{N}+\frac{(\Sigma I_0/N)^2}{S_{yy}}\right)\right]^{1/2}$$

where N is the number of data points,

$$S_{xx} = \Sigma\alpha^{-2} - (\Sigma\alpha^{-1})^2/N$$

$$S_{yy} = \Sigma I_0{}^2 - (\Sigma I_0)^2/N$$

$$S_{xy} = \Sigma(\alpha^{-1}I_0) - \Sigma\alpha^{-1}\Sigma I_0/N.$$

The tabulated *intensity* is I_0 while the plotted intensity is normalized to a maximum value of 5. All lengths are in micrometers.

SUPPLEMENTARY BIBLIOGRAPHY: GOLD-DOPED SILICON

These entries are a supplement to those in an earlier bibliography [1]. They either were found or were published after the previous bibliography was completed.

1962

Holonyak, N., Jr., Double Injection Diodes and Related DI Phenomena in Semiconductors, *Proc. IRE* 50, 2421-2428 (1962).

1965

Lauritzen, P. O., Low-Frequency Generation Noise in Junction Field Effect Transistors, *Solid-State Electronics* 8, 41-58 (1965).

1966

Anantharaman, T. R., Luo, H. L., and Klement, W., Jr., Formation of New Intermetallic Phases in Binary Eutectic Systems by Drastic Undercooling of the Melt, *Nature* 210, 1040-1041 (1966).

Aspnes, D. E., and Handler, P., Surface States on Cleaved (111) Silicon Surfaces, *Surface Sci.* 4, 353-380 (1966).

Moore, J. S., Penchina, C. M., Holonyak, N., Jr., Sirkis, M. D., and Yamada, T., Electrical Oscillations in Silicon Compensated with Deep Levels, *J. Appl. Phys.* 37, 2009-2013 (1966).

1967

Nassibian, A. G., Effect of Gold on Surface Properties and Leakage Current of MOS Transistors, *Solid-State Electronics* 10, 891-896 (1967).

1968

Güttler, G., and Queisser, H. J., Impurity Photovoltaic Effect in Silicon, *Proc. 7th Photovoltaic Specialists Conference*, Pasadena, California, 1968, pp. 1-8 (IEEE, New York, 1968).

Lambert, J. L., and Reese, M., The Gettering of Gold and Copper from Silicon, *Solid-State Electronics* 11, 1055-1061 (1968).

Wu, S. Y., Theory of the Generation-Recombination Noise in MOS Transistors, *Solid-State Electronics* 11, 25-32 (1968).

1969

Bishop, H. E., and Rivière, J. C., Segregation of Gold to the Silicon (111) Surface Observed by Auger Emission Spectroscopy and by LEED, *Brit. J. Appl. Phys. (J. Phys. D)* 2, 1635-1642 (1969).

Forbes, L., and Sah, C. T., Application of the Distributed Equilibrium Equivalent Circuit Model to Semiconductor Junctions, *IEEE Trans. Electron Devices* ED-16, 1036-1041 (1969).

Fu, H. S., and Sah, C. T., Lumped Model Analysis of the Low Frequency Generation Noise in Gold-Doped Silicon Junction-Gate Field-Effect Transistors, *Solid-State Electronics* 12, 605-618 (1969).

Güttler, G., and Queisser, H. J., Photovoltaic Effect of Gold in Silicon, *J. Appl. Phys.* 40, 4994-4995 (1969).

Sah, C. T., Rosier, L. L., and Forbes, L., Low-Temperature High-Frequency Capacitance Measurements of Deep- and Shallow-Level Impurity Center Concentrations, *Appl. Phys. Letters* 15, 161-164 (1969).

Yau, L. D., and Sah, C. T., Theory and Experiments of Low-Frequency Generation-Recombination Noise in MOS Transistors, *IEEE Trans. Electron Devices* ED-16, 170-177 (1969).

1970

Baykowski, J., Influence of Gold in Silicon on Electrical Properties of Epiplanar Transistors, *Electron Technol.* (Poland) 3, No. 4, 21-31 (1970).

Bisio, G. R., and Chiabrera, A. E., Recombination Waves in Au-Doped Si, *Appl. Phys. Letters* 16, 181-185 (1970).

Deuling, H. J., Double Injection Currents in Long *p-i-n* Diodes with One Trapping Level, *J. Appl. Phys.* 41, 2179-2184 (1970).

Grigor'ev, V. K., Muzyukin, L. P., Murygin, V. I., and Stafeev, V. I., Transient Processes in Long Diodes Made of Compensated Silicon, *Soviet Phys. Semiconductors* 4, 831-832 (1970-71).

Koifman, A. I., and Niyazova, O. R., Method for the Determination of Diffusion Profiles, *Soviet Phys. Semiconductors* 3, 1173-1174 (1969-70).

Lemke, H., and Müller, G. O., Time Dependence of Space Charge Limited Currents in Gold-Doped *p*-Si, *Phys. Status Solidi A* 1, 287-295 (1970).

Ogawa, T., Yatsuo, T., and Kamei, T., On Determination of Gold Trap Concentration in Diffused Silicon *p-n* Junctions, *Japan. J. Appl. Phys.* 9, 81-89 (1970).

Zwicker, H. R., Streetman, B. G., Andrews, A. M., and Deuling, H. J., Double Injection in Au-Doped Si *p-π-n* Diodes, *Appl. Phys. Letters* 16, 63-66 (1970).

Zyuz', L. N., Kiv, A. E., Niyazova, O. R., and Umarova, F. T., Photostimulated Diffusion in Silicon, *JETP Letters* 12, 147-149 (1970).

1971

Antognetti, P., Chiabrera, A., and Ridella, S., Recombination Wave Diode, *Solid-State Electronics* 14, 1123-1135 (1971).

Antognetti, P., Chiabrera, A., and Ridella, S., New Instability Criterion for Recombination Wave Diodes, *Appl. Phys. Letters* 18, 544-546 (1971).

Brotherton, S. D., Electrical Properties of Gold at the Silicon-Dielectric Interface, *J. Appl. Phys.* 42, 2085-2094 (1971).

EerNisse, E. P., Accurate Capacitance Calculations for *PN* Junctions Containing Traps, *Appl. Phys. Letters* 18, 183-186 (1971).

Klimkova, O. A., and Niyazova, O. R., Radiation-Accelerated Diffusion of Gold in Silicon, *Soviet Phys. Solid State* 12, 1760-1761 (1970-71).

Muzyukin, L. P., Murygin, V. I., Stafeev, V. I., and Tkachev, V. A., Impedance of a *p-i-n* Structure Made of Compensated Silicon, *Soviet Phys. Semiconductors* 5, 934-938 (1971-72).

Narusawa, T., Sakurai, T., and Hayakawa, K., Auger Electron Emission from Gold Deposited on Silicon (111) Surface, *Japan. J. Appl. Phys.* 10, 280-281 (1971).

Nassibian, A. G., and Sproul, M. E., Temperature Dependence of Gold-Doped MOSFET Devices, *Proc. Inst. Radio Electron. Eng. Aust.* 32, 239-247 (1971).

Taguchi, T., and Nakashima, K., Effect of Gold on the Anneal in Electron-Irradiated *p*-Type Si, *J. Phys. Soc. Jap.* 31, 955 (1971).

Weber, W. H., Elliott, R. S., and Cederquist, A. L., Small-Signal Transient Double Injection in Semiconductors Heavily Doped with Deep Traps, *J. Appl. Phys.* 42, 2497-2501 (1971).

Weber, W. H., and Ford, G. W., Space-Charge Recombination Oscillations in Double-Injection Structures, *Appl. Phys. Letters* 18, 241-244 (1971).

Wenaas, E. P., Leadon, R. E., Naber, J. A., and Mallon, C. E., Recombination Lifetimes in Gold-Doped *p*-Type Silicon, *J. Appl. Phys.* 42, 2893-2903 (1971).

Zarif'yants, Z. A., and Milevskii, L. S., Growth of Defect Loops in Dislocation-Free Silicon Single-Crystals, *Soviet Phys. Crystallogr.* 16, 493-497 (1971-72).

1972

Anthony, T. R., and Cline, H. E., Thermomigration of Gold-Rich Droplets in Silicon, *J. Appl. Phys.* 43, 2473-2476 (1972).

Antognetti, P., Chiabrera, A., and Ridella, S., Recombination Instabilities in Semiconductors Doped with Deep Two-Level Traps, *J. Appl. Phys.* 43, 4676-4680 (1972).

Badalov, A. Z., Kinetics of Precipitation of a Solid Solution of Gold in *n*-Type Silicon, *Soviet Phys. Semiconductors* 6, 685-687 (1972-73).

Badalov, A. Z., Belyakov, L. V., and Schuman, V. B., Absorption of Radiation in High-Resistivity Si: Au, *Soviet Phys. Semiconductors* 6, 809-810 (1972-73).

Berman, L. S., Barrier Capacitance of Silicon Diodes with Gold Impurities in the Base, *Soviet Phys. Semiconductors* 6, 285-288 (1972-73).

Bilenko, D. I., Zharkova, É. A., and Khasina, E. I., Transmission of Infrared Radiation by Gold-Doped Silicon Diodes, *Soviet Phys. Semiconductors* 6, 820-821 (1972-73).

Brotherton, S. D., and Rogers, T. L., Influence of Dislocations on Gold Diffusion into Thin Silicon Slices, *Solid-State Electronics* 15, 853-860 (1972).

Buck, T. M., Pickar, K. A., Poate, J. M., and Hsieh, C.-M., Gettering Rates of Various Fast-Diffusing Metal Impurities at Ion-Damaged Layers on Silicon, *Appl. Phys. Letters* 21, 485-487 (1972).

Buehler, M. G., Impurity Centers in *p-n* Junctions Determined from Shifts in the Thermally Stimulated Current and Capacitance Response with Heating Rate, *Solid-State Electronics* 15, 69-79 (1972).

Kleinpenning, Th. G. M., Impedance and G-R Noise of *n*-Type Gold-Doped Silicon under Space-Charge Conditions, *Physica* 58, 245-262 (1972).

Koifman, A. I., and Niyazova, O. R., Reactor Irradiation Enhanced Hetero-Diffusion in Silicon, *Phys. Status Solidi A* 10, 59-65 (1972).

McCombs, A. E., Jr., and Milnes, A. G., Impact Ionization of Deep-Impurities (In, Ni, Au) in Silicon, *Int. J. Electronics* 32, 361-376 (1972).

Parrillo, L. C., and Johnson, W. C., Acceptor State of Gold in Silicon-Resolution of an Anomaly, *Appl. Phys. Letters* 20, 104-106 (1972).

Sah, C. T., Chan, W. W., Fu, H. S., and Walker, J. W., Thermally Stimulated Capacitance (TSCAP) in *p-n* Junctions, *Appl. Phys. Letters* 20, 193-195 (1972).

Schuman, V. B., Absorption Spectrum of Si: Au, *Soviet Phys. Semiconductors* 6, 813-815 (1972-73).

Weber, W. H., and Ford, G. W., Instabilities and Small-Signal Response of Double Injection Structures with Deep Traps, *Solid-State Electronics* 15, 1277-1292 (1972).

Yau, L. D., and Sah. C. T., Measurement of Trapped-Minority-Carrier Thermal Emission Rates from Au, Ag, and Co Traps in Silicon, *Appl. Phys. Letters* 21, 157-158 (1972).

Yoshida, M., and Hirota, S., Reflection Electron Diffraction of Gold-Diffused Silicon, *Japan. J. Appl. Phys.* 11, 917-918 (1972).

Zohta, Y., Frequency Response of Gold Impurity Centers in the Depletion Layer of Reverse-Biased Silicon p^+n Junctions, *J. Appl. Phys.* 43, 1713-1716 (1972).

REFERENCE

1. Thurber, W. R., and Bullis, W. M., Resistivity and Carrier Lifetime in Gold-Doped Silicon, Air Force Cambridge Research Laboratories Report AFCRL-72-0076 (January 31, 1972). Available from National Technical Information Service, Springfield, Virginia 22151, Accession Number AD 740592.

FORM NBS-114A (1-71)

U.S. DEPT. OF COMM. BIBLIOGRAPHIC DATA SHEET	1. PUBLICATION OR REPORT NO. AFCRL-TR-73-0107	2. Gov't Accession No.	3. Recipient's Accession No. NBSIR-73-128

4. TITLE AND SUBTITLE RESISTIVITY AND CARRIER LIFETIME IN GOLD-DOPED SILICON.	5. Publication Date 6. Performing Organization Code
7. AUTHOR(S) W. Robert Thurber, David C. Lewis, and W. Murray Bullis	8. Performing Organization
9. PERFORMING ORGANIZATION NAME AND ADDRESS NATIONAL BUREAU OF STANDARDS DEPARTMENT OF COMMERCE WASHINGTON, D.C. 20234	10. Project/Task/Work Unit No. 6096-04-01 11. Contract/Grant No. PRO Y-72-873
12. Sponsoring Organization Name and Address AF Cambridge Research Laboratories (LQ) L. G. Hanscom Field Bedford, Massachusetts 01730	13. Type of Report & Period Covered Final 1 Jan. - 31 Dec. 1972 14. Sponsoring Agency Code

15. SUPPLEMENTARY NOTES Performed as part of Joint Program on Methods of Measurement for Semiconductor Materials, Process Control, and Devices with additional support from NBS (cost center 4251126).

16. ABSTRACT (A 200-word or less factual summary of most significant information. If document includes a significant bibliography or literature survey, mention it here.) This report describes the current status of a continuing study of the electrical properties of gold-doped silicon. Room Temperature resistivity and Hall effect measurements were made on many sets of gold-diffused boron- or phosphorus-doped silicon wafers for a wide range of initial resistivities of both types. The general suitability of the proposed model was verified although an apparent discrepancy still remains between total and electrically active gold as confirmed by resistivity data as a function of gold density for phosphorus-doped silicon. Electrical measurements were made to study the activation energies of the gold donor and acceptor. In addition the activation energy of the gold-coupled shallow acceptor in the proposed model was observed. The values found were in good agreement with other reported observations of these levels. In the application of the surface photovoltage method to the measurement of minority carrier lifetime, it was found that the optical absorption coefficients needed in the analysis of the data were dependent on the heat treatment given to the specimen. The uncertainty in diffusion length was determined to be about 2 μm which placed an effective lower limit on lifetime measurements of about 15 ns in *p*-type and about 50 ns in *n*-type silicon. An analysis of the use of the surface photovoltage method for lifetime measurements in thin epitaxial layers is included as an appendix. The reverse recovery (RR) technique for measuring lifetime was examined and it was observed that the dependence of diode storage time on the ratio of forward to reverse current varied with the base width of the diode studied. While theory and experiment for open circuit voltage decay (OCVD) were in agreement for long base width diodes, correlation for short base diodes was less satisfactory; this study is continuing. Both the RR and OCVD techniques give the same value of lifetime for long base diodes, but agreement for short base diodes is not as good. Additional entries are included as a supplement to an earlier bibliography on the properties of gold-doped silicon.

17. KEY WORDS (Alphabetical order, separated by semicolons) Carrier lifetime; gold-doped silicon; resistivity; semiconductor characterization; silicon.

18. AVAILABILITY STATEMENT	19. SECURITY CLASS (THIS REPORT)	21. NO. OF PAGES
[X] UNLIMITED.	UNCLASSIFIED	59
[ ] FOR OFFICIAL DISTRIBUTION. DO NOT RELEASE TO NTIS.	20. SECURITY CLASS (THIS PAGE) UNCLASSIFIED	22. Price